# Generalizations of the Kerr-Newman solution

# Contents

# 1 Topics

- Generalizations of the Kerr-Newman solution
- Properties of Kerr-Newman spacetimes
- Quadrupolar metrics

## 1.1 ICRANet Participants

- Roy P. Kerr
- Hernando Quevedo
- Jorge A. Rueda
- Remo Ruffini

## 1.2 Ongoing collaborations

- Medeu Abishev (Kazakh National University - KazNU, Kazakhstan)
- Nurzada Beissen (Taraz State Pedagogical University, Kazakhstan)
- Kuantay Boshkayev (Kazakh National University - KazNU, Kazakhstan)
- Antonio C. Gutierrez (Industrial University of Santander, Colombia)
- Orlando Luongo (University of Naples, Italy)
- Daniela Pugliese (Silesian University in Opava, Czech Republic)
- Saken Toktarbay (Kazakh National University - KazNU, Kazakhstan)

## 1.3 Students

- Jesús Anaya, (UNAM, PhD, Mexico)
- Aizhan Mansurova (KazNU PhD, Kazakhstan)
- Sasha Zaldivar (UNAM PhD, Mexico)
- Carlos Romero (UNAM PhD, Mexico)
- Elly Bayona (UNAM PhD, Mexico)
- Luis Cedeño (UNAM PhD, Mexico)
- José M. Ladino (UNAM PhD, Mexico)

# 2 Brief description

One of the most important metrics in general relativity is the Kerr-Newman solution that describes the gravitational and electromagnetic fields of a rotating charged mass. In fact, it is widely believed that this metric can be used only in the case of black holes because its possesses a limited number of multipole moments, namely, the monopoles of mass and charge and the angular momentum dipole. All the higher multipole moments can be expressed in terms of these three independent moments. For instance, the quadrupole moment is proportional to the angular momentum dipole, which, in turn, contains the mass monopole.

Astrophysical compact objects, however, are characterized by shape deformations that can be described only by means of higher independent moments. For instance, even a small deviation from spherical symmetry would generate a quadrupole moment that should be independent of the rotational properties of the body. Also, the moment of inertia of the system is expected to be related to the a rotational quadrupole moment. On the other hand, the rotation of a body is also expected to induce, in general, shape deformations that should be taken into account when considering the general set of multipole moments that are necessary for describing the corresponding gravitational field. Therefore, we expect that a general treatment of the gravitational field of compact objects implies the introduction of two independent sets of multipole moments, one related to the distribution of mass and its shape, and the second one associated to the moment of inertia and other rotational properties of the body. Furthermore, if the constituent particles of the mass distribution are endowed with electric charge, an additional set of electromagnetic multipole moments should be considered.

It follows that to attack the problem of describing the gravitational and electromagnetic fields of an arbitrary distribution of charged masses, it is necessary to derive and investigate new exact solutions of Einstein-Maxwell equations, which posses an infinite set of gravitational and electromagnetic multipole moments and contain the Kerr-Newman solution as special case.

We consider the circular motion of test particles in the gravitational field

of a rotating deformed object described by the Hartle-Thorne metric. This metric represents an approximate solution to the vacuum Einstein field equations, accurate to second order in the angular momentum $J$ and to first order in the mass quadrupole moment $Q$. We calculate the orbital parameters of neutral test particles on circular orbits (in accretion disks) such as angular velocity, $\Omega$, total energy, $E$, angular momentum, $L$, and radius of the innermost stable circular orbit, $R_{ISCO}$, as functions of the total mass, $M$, spin parameter, $j = J/M^2$ and quadrupole parameter, $q = Q/M^3$, of the source. We use the Novikov-Thorne-Page thin accretion disk model to investigate the characteristics of the disk. In particular, we analyze in detail the radiative flux, differential luminosity, and spectral luminosity of the accretion disk, which are the quantities that can be measured experimentally. We compare our results with those obtained in the literature for the Schwarzschild and Kerr metrics, and the $q$-metric. It turns out that the Hartle-Thorne metric and the Kerr metric lead to similar results for the predicted flux and the differential and spectral luminosities, whereas the q-metric predicts different values. We compare the predicted values of $M$, $j$, and $q$ with those of realistic neutron star models. Furthermore, we compare the values of $R_{ISCO}$ with the static and rotating radii of neutron stars.

# 3 Introduction

It is hard to overemphasize the importance of the Kerr geometry not only for general relativity itself, but also for the very fundamentals of physics. It assumes this position as being the most physically relevant rotating generalization of the static Schwarzschild geometry. Its charged counterpart, the Kerr-Newman solution, representing the exterior gravitational and electromagnetic fields of a charged rotating object, is an exact solution of the Einstein-Maxwell equations.

Its line element in Boyer–Lindquist coordinates can be written as

$$\begin{aligned} ds^2 &= \frac{r^2 - 2Mr + a^2 + Q^2}{r^2 + a^2\cos^2\theta}(dt - a\sin^2\theta d\varphi)^2 \\ &\quad - \frac{\sin^2\theta}{r^2 + a^2\cos^2\theta}[(r^2 + a^2)d\varphi - adt]^2 \\ &\quad - \frac{r^2 + a^2\cos^2\theta}{r^2 - 2Mr + a^2 + Q^2}dr^2 - (r^2 + a^2\cos^2\theta)d\theta^2\,, \end{aligned} \tag{3.0.1}$$

where $M$ is the total mass of the object, $a = J/M$ is the specific angular momentum, and $Q$ is the electric charge. In this particular coordinate system, the metric functions do not depend on the coordinates $t$ and $\phi$, indicating the existence of two Killing vector fields $\xi^I = \partial_t$ and $\xi^{II} = \partial_\varphi$ which represent the properties of stationarity and axial symmetry, respectively.

An important characteristic of this solution is that the source of gravity is surrounded by two horizons situated at a distance

$$r_\pm = M \pm \sqrt{M^2 - a^2 - Q^2} \tag{3.0.2}$$

from the origin of coordinates. Inside the interior horizon, $r_-$, a ring singularity is present which, however, cannot be observed by any observer situated outside the exterior horizon. If the condition $M^2 < a^2 + Q^2$ is satisfied, no horizons are present and the Kerr–Newman spacetime represents the exterior field of a naked singularity.

Despite of its fundamental importance in general relativity, and its theoretical and mathematical interest, this solution has not been especially useful for describing astrophysical phenomena, first of all, because observed astrophysical objects do not possess an appreciable net electric charge. Furthermore, the limiting Kerr metric takes into account the mass and the rotation, but does not consider the moment of inertia of the object. For astrophysical applications it is, therefore, necessary to use more general solutions with higher multipole moments which are due not only to the rotation of the body but also to its shape. This means that even in the limiting case of a static spacetime, a solution is needed that takes into account possible deviations from spherically symmetry.

# 4 The general static vacuum solution

In general relativity, stationary axisymmetric solutions of Einstein's equations (1) play a crucial role for the description of the gravitational field of astrophysical objects. In particular, the black hole solutions and their generalizations that include Maxwell fields are contained within this class.

This type of exact solutions has been the subject of intensive research during the past few decades. In particular, the number of know exact solutions drastically increased after Ernst (2) discovered an elegant representation of the field equations that made it possible to search for their symmetries. These studies lead finally to the development of solution generating techniques (1) which allow us to find new solutions, starting from a given seed solution. In particular, solutions with an arbitrary number of multipole moments for the mass and angular momentum were derived in (3) and used to describe the gravitational field of rotating axially symmetric distributions of mass.

The first analysis of stationary axially symmetric gravitational fields was carried out by Weyl (4) in 1917, soon after the formulation of general relativity. In particular, Weyl discovered that in the static limit the main part of the vacuum field equations reduces to a single linear differential equation. The corresponding general solution can be written in cylindrical coordinates as an infinite sum with arbitrary constant coefficients. A particular choice of the coefficients leads to the subset of asymptotically flat solutions which is the most interesting from a physical point of view. In this section we review the main properties of stationary axisymmetric gravitational fields. In particular, we show explicitly that the main field equations in vacuum can be represented as the equations of a nonlinear sigma model in which the base space is the 4-dimensional spacetime and the target space is a 2-dimensional conformally Euclidean space.

## 4.1 Line element and field equations

Although there exist in the literature many suitable coordinate systems, stationary axisymmetric gravitational fields are usually described in cylindric coordinates $(t, \rho, z, \varphi)$. Stationarity implies that $t$ can be chosen as the time coordinate and the metric does not depend on time, i.e. $\partial g_{\mu\nu}/\partial t = 0$. Consequently, the corresponding timelike Killing vector has the components $\delta^{\mu}_{t}$. A second Killing vector field is associated to the axial symmetry with respect to the axis $\rho = 0$. Then, choosing $\varphi$ as the azimuthal angle, the metric satisfies the conditions $\partial g_{\mu\nu}/\partial\varphi = 0$, and the components of the corresponding spacelike Killing vector are $\delta^{\mu}_{\varphi}$.

Using further the properties of stationarity and axial symmetry, together with the vacuum field equations, for a general metric of the form $g_{\mu\nu} = g_{\mu\nu}(\rho, z)$, it is possible to show that the most general line element for this type of gravitational fields can be written in the Weyl-Lewis-Papapetrou form as (4; 5; 6)

$$ds^2 = f(dt - \omega d\varphi)^2 - f^{-1}\left[e^{2\gamma}(d\rho^2 + dz^2) + \rho^2 d\varphi^2\right] , \tag{4.1.1}$$

where $f$, $\omega$ and $\gamma$ are functions of $\rho$ and $z$, only. After some rearrangements which include the introduction of a new function $\Omega = \Omega(\rho, z)$ by means of

$$\rho\partial_\rho\Omega = f^2\partial_z\omega , \qquad \rho\partial_z\Omega = -f^2\partial_\rho\omega , \tag{4.1.2}$$

the vacuum field equations $R_{\mu\nu} = 0$ can be shown to be equivalent to the following set of partial differential equations

$$\frac{1}{\rho}\partial_\rho(\rho\partial_\rho f) + \partial_z^2 f + \frac{1}{f}[(\partial_\rho\Omega)^2 + (\partial_z\Omega)^2 - (\partial_\rho f)^2 - (\partial_z f)^2] = 0 , \tag{4.1.3}$$

$$\frac{1}{\rho}\partial_\rho(\rho\partial_\rho\Omega) + \partial_z^2\Omega - \frac{2}{f}\left(\partial_\rho f\,\partial_\rho\Omega + \partial_z f\,\partial_z\Omega\right) = 0 , \tag{4.1.4}$$

$$\partial_\rho\gamma = \frac{\rho}{4f^2}\left[(\partial_\rho f)^2 + (\partial_\rho\Omega)^2 - (\partial_z f)^2 - (\partial_z\Omega)^2\right] , \tag{4.1.5}$$

$$\partial_z\gamma = \frac{\rho}{2f^2}\left(\partial_\rho f\,\partial_z f + \partial_\rho\Omega\,\partial_z\Omega\right) . \tag{4.1.6}$$

It is clear that the field equations for $\gamma$ can be integrated by quadratures,

once $f$ and $\Omega$ are known. For this reason, the equations (4.1.3) and (4.1.4) for $f$ and $\Omega$ are usually considered as the main field equations for stationary axisymmetric vacuum gravitational fields. In the following subsections we will focus on the analysis of the main field equations, only. It is interesting to mention that this set of equations can be geometrically interpreted in the context of nonlinear sigma models (17).

Let us consider the special case of static axisymmetric fields. This corresponds to metrics which, apart from being axially symmetric and independent of the time coordinate, are invariant with respect to the transformation $\varphi \to -\varphi$ (i.e. rotations with respect to the axis of symmetry are not allowed). Consequently, the corresponding line element is given by (4.1.1) with $\omega = 0$, and the field equations can be written as

$$\partial_\rho^2 \psi + \frac{1}{\rho}\partial_\rho \psi + \partial_z^2 \psi = 0 \,, \quad f = \exp(2\psi) \,, \tag{4.1.7}$$

$$\partial_\rho \gamma = \rho \left[ (\partial_\rho \psi)^2 - (\partial_z \psi)^2 \right] \,, \quad \partial_z \gamma = 2\rho \partial_\rho \psi \, \partial_z \psi \,. \tag{4.1.8}$$

We see that the main field equation (4.1.7) corresponds to the linear Laplace equation for the metric function $\psi$.

## 4.2 Static solution

The general solution of Laplace's equation is known and, if we demand additionally asymptotic flatness, we obtain the Weyl solution which can be written as (4; 1)

$$\psi = \sum_{n=0}^{\infty} \frac{a_n}{(\rho^2 + z^2)^{\frac{n+1}{2}}} P_n(\cos\theta) \,, \qquad \cos\theta = \frac{z}{\sqrt{\rho^2 + z^2}} \,, \tag{4.2.1}$$

where $a_n$ $(n = 0, 1, ...)$ are arbitrary constants, and $P_n(\cos\theta)$ represents the Legendre polynomials of degree $n$. The expression for the metric function $\gamma$ can be calculated by quadratures by using the set of first order differential equations (4.1.8). Then

$$\gamma = -\sum_{n,m=0}^{\infty} \frac{a_n a_m (n+1)(m+1)}{(n+m+2)(\rho^2 + z^2)^{\frac{n+m+2}{2}}} \left( P_n P_m - P_{n+1} P_{m+1} \right) \,. \tag{4.2.2}$$

Since this is the most general static, axisymmetric, asymptotically flat vacuum solution, it must contain all known solution of this class. In particular, one of the most interesting special solutions which is Schwarzschild's spherically symmetric black hole spacetime must be contained in this class. To see this, we must choose the constants $a_n$ in such a way that the infinite sum (4.2.1) converges to the Schwarzschild solution in cylindric coordinates. But, or course, this representation is not the most appropriate to analyze the interesting physical properties of Schwarzschild's metric.

In fact, it turns out that to investigate the properties of solutions with multipole moments it is more convenient to use prolate spheroidal coordinates $(t, x, y, \varphi)$ in which the line element can be written as

$$ds^2 = f dt^2 - \frac{\sigma^2}{f}\left[e^{2\gamma}(x^2-y^2)\left(\frac{dx^2}{x^2-1}+\frac{dy^2}{1-y^2}\right)+(x^2-1)(1-y^2)d\varphi^2\right]$$

where

$$x = \frac{r_+ + r_-}{2\sigma}\,, \quad (x^2 \geq 1), \quad y = \frac{r_+ - r_-}{2\sigma}\,, \quad (y^2 \leq 1) \tag{4.2.3}$$

$$r_\pm^2 = \rho^2 + (z \pm \sigma)^2\,, \quad \sigma = const\,, \tag{4.2.4}$$

and the metric functions are $f$, $\omega$, and $\gamma$ depend on $x$ and $y$, only. In this coordinate system, the general static solution which is also asymptotically flat can be expressed as

$$f = \exp(2\psi)\,, \quad \psi = \sum_{n=0}^{\infty}(-1)^{n+1} q_n P_n(y) Q_n(x)\,, \quad q_n = const$$

where $P_n(y)$ are the Legendre polynomials, and $Q_n(x)$ are the Legendre functions of second kind. In particular,

$$P_0 = 1, \quad P_1 = y, \quad P_2 = \frac{1}{2}(3y^2-1)\,, ...$$

$$Q_0 = \frac{1}{2}\ln\frac{x+1}{x-1}\,, \quad Q_1 = \frac{1}{2}x\ln\frac{x+1}{x-1} - 1\,,$$
$$Q_2 = \frac{1}{2}(3x^2-1)\ln\frac{x+1}{x-1} - \frac{3}{2}x\,, ...$$

The corresponding function $\gamma$ can be calculated by quadratures and its general expression has been explicitly derived in (3). The most important special cases contained in this general solution are the Schwarzschild metric

$$\psi = -q_0 P_0(y) Q_0(x) \,, \quad \gamma = \frac{1}{2} \ln \frac{x^2 - 1}{x^2 - y^2} \,,$$

and the Erez-Rosen metric (9)

$$\psi = -q_0 P_0(y) Q_0(x) - q_2 P_2(y) Q_2(x) \,, \quad \gamma = \frac{1}{2} \ln \frac{x^2 - 1}{x^2 - y^2} + .... \,$$

In the last case, the constant parameter $q_2$ turns out to determine the quadrupole moment. In general, the constants $q_n$ represent an infinite set of parameters that determines an infinite set of mass multipole moments. The parameters $q_n$ represent the deviation of the mass distribution from the ideal spherical symmetry. It is interesting to mention that if demand the additional symmetry with respect to the equatorial plane $\theta = \pi/2$, it can be shown that all odd parameters $q_{2k+1}$, $k = 0, 1, ...$ should vanish. This is an additional symmetry condition that reduces the form of the resulting metric.

# 5 Stationary generalization

The solution generating techniques (12) can be applied, in particular, to any static seed solution in order to obtain the corresponding stationary generalization. One of the most powerful techniques is the inverse method (ISM) developed by Belinski and Zakharov (13). We used a particular case of the ISM, which is known as the Hoenselaers–Kinnersley-Xanthopoulos (HKX) transformation to derive the stationary generalization of the general static solution in prolate spheroidal coordinates.

## 5.1 Ernst representation

In the general stationary case ($\omega \neq 0$) with line element

$$\begin{aligned} & ds^2 = f(dt - \omega d\varphi)^2 \\ - \; & \frac{\sigma^2}{f}\left[e^{2\gamma}(x^2-y^2)\left(\frac{dx^2}{x^2-1}+\frac{dy^2}{1-y^2}\right)+(x^2-1)(1-y^2)d\varphi^2\right] \end{aligned}$$

it is useful to introduce the the Ernst potentials

$$E = f + i\Omega\,, \quad \xi = \frac{1-E}{1+E}\,,$$

where the function $\Omega$ is now determined by the equations

$$\sigma(x^2-1)\Omega_x = f^2\omega_y\,, \quad \sigma(1-y^2)\Omega_y = -f^2\omega_x\,.$$

Then, the main field equations can be represented in a compact and symmetric form:

$$(\xi\xi^*-1)\left\{[(x^2-1)\xi_x]_x + [(1-y^2)\xi_y]_y\right\} = 2\xi^*[(x^2-1)\xi_x^2 + (1-y^2)\xi_y^2]\,.$$

This equation is invariant with respect to the transformation $x \leftrightarrow y$. Then, since the particular solution

$$\xi = \frac{1}{x} \rightarrow \Omega = 0 \rightarrow \omega = 0 \rightarrow \gamma = \frac{1}{2} \ln \frac{x^2 - 1}{x^2 - y^2}$$

represents the Schwarzschild spacetime, the choice $\xi^{-1} = y$ is also an exact solution. Furthermore, if we take the linear combination $\xi^{-1} = c_1 x + c_2 y$ and introduce it into the field equation, we obtain the new solution

$$\xi^{-1} = \frac{\sigma}{M} x + i \frac{a}{M} y \, , \; \sigma = \sqrt{M^2 - a^2} \, ,$$

which corresponds to the Kerr metric in prolate spheroidal coordinates.

In the case of the Einstein-Maxwell theory, the main field equations can be expressed as

$$(\xi\xi^* - \mathcal{F}\mathcal{F}^* - 1)\nabla^2 \xi = 2(\xi^* \nabla \xi - \mathcal{F}^* \nabla \mathcal{F}) \nabla \xi \, ,$$

$$(\xi\xi^* - \mathcal{F}\mathcal{F}^* - 1)\nabla^2 \mathcal{F} = 2(\xi^* \nabla \xi - \mathcal{F}^* \nabla \mathcal{F}) \nabla \mathcal{F}$$

where $\nabla$ represents the gradient operator in prolate spheroidal coordinates. Moreover, the gravitational potential $\xi$ and the electromagnetic $\mathcal{F}$ Ernst potential are defined as

$$\xi = \frac{1 - f - i\Omega}{1 + f + i\Omega} \, , \quad \mathcal{F} = 2 \frac{\Phi}{1 + f + i\Omega} \, .$$

The potential $\Phi$ can be shown to be determined uniquely by the electromagnetic potentials $A_t$ and $A_\varphi$ One can show that if $\xi_0$ is a vacuum solution, then the new potential

$$\xi = \xi_0 \sqrt{1 - e^2}$$

represents a solution of the Einstein-Maxwell equations with effective electric charge $e$. This transformation is known in the literature as the Harrison transformation (10). Accordingly, the Kerr–Newman solution in this representation acquires the simple form

$$\xi = \frac{\sqrt{1 - e^2}}{\frac{\sigma}{M} x + i \frac{a}{M} y} \, , \qquad e = \frac{Q}{M} \, , \qquad \sigma = \sqrt{M^2 - a^2 - Q^2} \, .$$

In this way, it is very easy to generalize any vacuum solution to include the case of electric charge. More general transformations of this type can be used in order to generate solutions with any desired set of gravitational and electromagnetic multipole moments (3).

## 5.2 Representation as a nonlinear sigma model

Consider two (pseudo)-Riemannian manifolds $(M, \gamma)$ and $(N, G)$ of dimension $m$ and $n$, respectively. Let $M$ be coordinatized by $x^a$, and $N$ by $X^\mu$, so that the metrics on $M$ and $N$ can be, in general, smooth functions of the corresponding coordinates, i.e., $\gamma = \gamma(x)$ and $G = G(X)$. A harmonic map is a smooth map $X : M \to N$, or in coordinates $X : x \longmapsto X$ so that $X$ becomes a function of $x$, and the $X$'s satisfy the motion equations following from the action (14)

$$S = \int d^m x \sqrt{|\gamma|}\, \gamma^{ab}(x)\, \partial_a X^\mu\, \partial_b X^\nu\, G_{\mu\nu}(X)\,, \tag{5.2.1}$$

which sometimes is called the "energy" of the harmonic map $X$. The straightforward variation of $S$ with respect to $X^\mu$ leads to the motion equations

$$\frac{1}{\sqrt{|\gamma|}} \partial_b \left( \sqrt{|\gamma|} \gamma^{ab} \partial_a X^\mu \right) + \Gamma^\mu_{\ \nu\lambda}\, \gamma^{ab}\, \partial_a X^\nu\, \partial_b X^\lambda = 0\,, \tag{5.2.2}$$

where $\Gamma^\mu_{\ \nu\lambda}$ are the Christoffel symbols associated to the metric $G_{\mu\nu}$ of the target space $N$. If $G_{\mu\nu}$ is a flat metric, one can choose Cartesian-like coordinates such that $G_{\mu\nu} = \eta_{\mu\nu} = diag(\pm 1, ..., \pm 1)$, the motion equations become linear, and the corresponding sigma model is linear. This is exactly the case of a bosonic string on a flat background in which the base space is the 2-dimensional string world-sheet. In this case the action (5.2.1) is usually referred to as the Polyakov action (16).

Consider now the case in which the base space $M$ is a stationary axisymmetric spacetime. Then, $\gamma^{ab}$, $a, b = 0, ..., 3$, can be chosen as the Weyl-Lewis-Papapetrou metric (4.1.1), i.e.

$$\gamma_{ab} = \begin{pmatrix} f & 0 & 0 & -f\omega \\ 0 & -f^{-1}e^{2k} & 0 & 0 \\ 0 & 0 & -f^{-1}e^{2k} & 0 \\ -f\omega & 0 & 0 & f\omega^2 - \rho^2 f^{-1} \end{pmatrix}. \tag{5.2.3}$$

Let the target space $N$ be 2-dimensional with metric $G_{\mu\nu} = (1/2)f^{-2}\delta_{\mu\nu}$, $\mu,\nu = 1,2$, and let the coordinates on $N$ be $X^\mu = (f,\Omega)$. Then, it is straightforward to show that the action (5.2.1) becomes

$$S = \int \mathcal{L}\, dtd\varphi d\rho dz\,, \qquad \mathcal{L} = \frac{\rho}{2f^2}\left[(\partial_\rho f)^2 + (\partial_z f)^2 + (\partial_\rho \Omega)^2 + (\partial_z \Omega)^2\right]\,, \tag{5.2.4}$$

and the corresponding motion equations (5.2.2) are identical to the main field equations (4.1.3) and (4.1.4).

Notice that the field equations can also be obtained from (5.2.4) by a direct variation with respect to $f$ and $\Omega$. This interesting result was obtained originally by Ernst (2), and is the starting point of what today is known as the Ernst representation of the field equations.

The above result shows that stationary axisymmetric gravitational fields can be described as a $(4 \to 2)-$nonlinear harmonic map, where the base space is the spacetime of the gravitational field and the target space corresponds to a 2-dimensional conformally Euclidean space. A further analysis of the target space shows that it can be interpreted as the quotient space $SL(2,R)/SO(2)$, and the Lagrangian (5.2.4) can be written explicitly (17) in terms of the generators of the Lie group $SL(2,R)$. Harmonic maps in which the target space is a quotient space are usually known as nonlinear sigma models (14).

The form of the Lagrangian (5.2.4) with two gravitational field variables, $f$ and $\Omega$, depending on two coordinates, $\rho$ and $z$, suggests a representation as a harmonic map with a 2-dimensional base space. In string theory, this is an important fact that allows one to use the conformal invariance of the base space metric to find an adequate representation for the set of classical solutions. This, in turn, facilitates the application of the canonical quantization procedure. Unfortunately, this is not possible for the Lagrangian (5.2.4). Indeed, if we consider $\gamma^{ab}$ as a 2-dimensional metric that depends on the parameters $\rho$ and $z$, the diagonal form of the Lagrangian (5.2.4) implies that $\sqrt{|\gamma|}\gamma^{ab} = \delta^{ab}$. Clearly, this choice is not compatible with the factor $\rho$ in front of the Lagrangian. Therefore, the reduced gravitational Lagrangian (5.2.4) cannot be interpreted as corresponding to a $(2 \to n)$-harmonic map. Nevertheless, we will show in the next section that a modification of the definition of harmonic maps allows us to "absorb" the unpleasant factor $\rho$ in the metric of the target space, and to use all the advantages of a 2-dimensional base space.

Notice that the representation of stationary fields as a nonlinear sigma model becomes degenerate in the limiting case of static fields. Indeed, the underlying geometric structure of the $SL(2,R)/SO(2)$ nonlinear sigma models requires that the target space be 2-dimensional, a condition which is not satisfied by static fields. We will see below that by using a dimensional extension of generalized sigma models, it will be possible to treat the special static case, without affecting the underlying geometric structure.

The analysis performed in this section for stationary axisymmetric fields can be generalized to include any gravitational field containing two commuting Killing vector fields (1). This is due to the fact that for this class of gravitational fields it is always possible to find the corresponding Ernst representation in which the Lagrangian contains only two gravitational variables which depend on only two spacetime coordinates.

## 5.3 Representation as a generalized harmonic map

Consider two (pseudo-)Riemannian manifolds $(M,\gamma)$ and $(N,G)$ of dimension $m$ and $n$, respectively. Let $x^a$ and $X^\mu$ be coordinates on $M$ and $N$, respectively. This coordinatization implies that in general the metrics $\gamma$ and $G$ become functions of the corresponding coordinates. Let us assume that not only $\gamma$ but also $G$ can explicitly depend on the coordinates $x^a$, i.e. let $\gamma=\gamma(x)$ and $G=G(X,x)$. This simple assumption is the main aspect of our generalization which, as we will see, lead to new and nontrivial results.

A smooth map $X: M\to N$ will be called an $(m\to n)-$generalized harmonic map if it satisfies the Euler-Lagrange equations

$$\frac{1}{\sqrt{|\gamma|}}\partial_b\left(\sqrt{|\gamma|}\gamma^{ab}\partial_a X^\mu\right)+\Gamma^\mu_{\nu\lambda}\,\gamma^{ab}\,\partial_a X^\nu\partial_b X^\lambda+G^{\mu\lambda}\gamma^{ab}\,\partial_a X^\nu\,\partial_b G_{\lambda\nu}=0\,, \tag{5.3.1}$$

which follow from the variation of the generalized action

$$S=\int d^m x\sqrt{|\gamma|}\,\gamma^{ab}(x)\,\partial_a X^\mu\partial_b X^\nu G_{\mu\nu}(X,x)\,, \tag{5.3.2}$$

with respect to the fields $X^\mu$. Here the Christoffel symbols, determined by the metric $G_{\mu\nu}$, are calculated in the standard manner, without considering the explicit dependence on $x$. Notice that the new ingredient in this generalized definition of harmonic maps, i.e., the term $G_{\mu\nu}(X,x)$ in the Lagrangian

density implies that we are taking into account the "interaction" between the base space $M$ and the target space $N$. This interaction leads to an extra term in the motion equations, as can be seen in (5.3.1). It turns out that this interaction is the result of the effective presence of the gravitational field.

Notice that the limiting case of generalized linear harmonic maps is much more complicated than in the standard case. Indeed, for the motion equations (5.3.1) to become linear it is necessary that the conditions

$$\gamma^{ab}(\Gamma^{\mu}_{\ \nu\lambda}\ \partial_b X^{\lambda} + G^{\mu\lambda}\,\partial_b G_{\lambda\nu})\partial_a X^{\nu} = 0\,, \tag{5.3.3}$$

be satisfied. One could search for a solution in which each term vanishes separately. The choice of a (pseudo-)Euclidean target metric $G_{\mu\nu} = \eta_{\mu\nu}$, which would imply $\Gamma^{\mu}_{\ \nu\lambda} = 0$, is not allowed, because it would contradict the assumption $\partial_b G_{\mu\nu} \neq 0$. Nevertheless, a flat background metric in curvilinear coordinates could be chosen such that the assumption $G^{\mu\lambda}\partial_b G_{\mu\nu} = 0$ is fulfilled, but in this case $\Gamma^{\mu}_{\ \nu\lambda} \neq 0$ and (5.3.3) cannot be satisfied. In the general case of a curved target metric, conditions (5.3.3) represent a system of $m$ first order nonlinear partial differential equations for $G_{\mu\nu}$. Solutions to this system would represent linear generalized harmonic maps. The complexity of this system suggests that this special type of maps is not common.

As we mentioned before, the generalized action (5.3.2) includes an interaction between the base space $N$ and the target space $M$, reflected on the fact that $G_{\mu\nu}$ depends explicitly on the coordinates of the base space. Clearly, this interaction must affect the conservation laws of the physical systems we attempt to describe by means of generalized harmonic maps. To see this explicitly we calculate the covariant derivative of the generalized Lagrangian density

$$\mathcal{L} = \sqrt{|\gamma|}\,\gamma^{ab}(x)\,\partial_a\, X^{\mu}\partial_b X^{\nu} G_{\mu\nu}(X,x)\,, \tag{5.3.4}$$

and replace in the result the corresponding motion equations (5.3.1). Then, the final result can be written as

$$\nabla_b \widetilde{T}_a^{\ b} = -\frac{\partial \mathcal{L}}{\partial x^a} \tag{5.3.5}$$

where $\widetilde{T}_a{}^b$ represents the canonical energy-momentum tensor

$$\widetilde{T}_a{}^b = \frac{\partial \mathcal{L}}{\partial(\partial_b X^\mu)}(\partial_a X^\mu) - \delta_a^b \mathcal{L} = 2\sqrt{\gamma} G_{\mu\nu}\left(\gamma^{bc}\partial_a X^\mu\, \partial_c X^\nu - \frac{1}{2}\delta_a^b \gamma^{cd}\partial_c X^\mu\, \partial_d X^\nu\right). \tag{5.3.6}$$

The standard conservation law is recovered only when the Lagrangian does not depend explicitly on the coordinates of the base space. Even if we choose a flat base space $\gamma_{ab} = \eta_{ab}$, the explicit dependence of the metric of the target space $G_{\mu\nu}(X, x)$ on $x$ generates a term that violates the standard conservation law. This term is due to the interaction between the base space and the target space which, consequently, is one of the main characteristics of the generalized harmonic maps introduced in this work.

An alternative and more general definition of the energy-momentum tensor is by means of the variation of the Lagrangian density with respect to the metric of the base space, i.e.

$$T_{ab} = \frac{\delta \mathcal{L}}{\delta \gamma^{ab}}\,. \tag{5.3.7}$$

A straightforward computation shows that for the action under consideration here we have that $\widetilde{T}_{ab} = 2T_{ab}$ so that the generalized conservation law (5.3.5) can be written as

$$\nabla_b T_a{}^b + \frac{1}{2}\frac{\partial \mathcal{L}}{\partial x^a} = 0\,. \tag{5.3.8}$$

For a given metric on the base space, this represents in general a system of $m$ differential equations for the "fields" $X^\mu$ which must be satisfied "on-shell".

If the base space is 2-dimensional, we can use a reparametrization of $x$ to choose a conformally flat metric, and the invariance of the Lagrangian density under arbitrary Weyl transformations to show that the energy-momentum tensor is traceless, $T_a{}^a = 0$.

In Section 5.1 we described stationary, axially symmetric, gravitational fields as a $(4 \to 2)-$nonlinear sigma model. There it was pointed out the convenience of having a 2-dimensional base space in analogy with string theory. Now we will show that this can be done by using the generalized harmonic maps defined above.

Consider a $(2 \to 2)-$generalized harmonic map. Let $x^a = (\rho, z)$ be the coordinates on the base space $M$, and $X^\mu = (f, \Omega)$ the coordinates on the target space $N$. In the base space we choose a flat metric and in the target

space a conformally flat metric, i.e.

$$\gamma_{ab} = \delta_{ab} \qquad \text{and} \qquad G_{\mu\nu} = \frac{\rho}{2f^2}\delta_{\mu\nu} \qquad (a,b = 1,2;\ \mu,\nu = 1,2). \tag{5.3.9}$$

A straightforward computation shows that the generalized Lagrangian (5.3.4) coincides with the Lagrangian (5.2.4) for stationary axisymetric fields, and that the equations of motion (5.3.1) generate the main field equations (4.1.3) and (4.1.4).

For the sake of completeness we calculate the components of the energy-momentum tensor $T_{ab} = \delta\mathcal{L}/\delta\gamma^{ab}$. Then

$$T_{\rho\rho} = -T_{zz} = \frac{\rho}{4f^2}\left[(\partial_\rho f)^2 + (\partial_\rho \Omega)^2 - (\partial_z f)^2 - (\partial_z \Omega)^2\right], \tag{5.3.10}$$

$$T_{\rho z} = \frac{\rho}{2f^2}\left(\partial_\rho f\, \partial_z f + \partial_\rho \Omega\ \partial_z \Omega\right). \tag{5.3.11}$$

This tensor is traceless due to the fact that the base space is 2-dimensional. It satisfies the generalized conservation law (5.3.8) on-shell:

$$\frac{dT_{\rho\rho}}{d\rho} + \frac{dT_{\rho z}}{dz} + \frac{1}{2}\frac{\partial\mathcal{L}}{\partial\rho} = 0\,, \tag{5.3.12}$$

$$\frac{dT_{\rho z}}{d\rho} - \frac{dT_{\rho\rho}}{dz} = 0\,. \tag{5.3.13}$$

Incidentally, the last equation coincides with the integrability condition for the metric function $k$, which is identically satisfied by virtue of the main field equations. In fact, as can be seen from Eqs.(4.1.5,4.1.6) and (5.3.10,5.3.11), the components of the energy-momentum tensor satisfy the relationships $T_{\rho\rho} = \partial_\rho k$ and $T_{\rho z} = \partial_z k$, so that the conservation law (5.3.13) becomes an identity. Although we have eliminated from the starting Lagrangian (5.2.4) the variable $k$ by applying a Legendre transformation on the Einstein-Hilbert Lagrangian (see (17)) for this type of gravitational fields, the formalism of generalized harmonic maps seems to retain the information about $k$ at the level of the generalized conservation law.

The above results show that stationary axisymmetric spacetimes can be represented as a $(2 \to 2)-$generalized harmonic map with metrics given as in (5.3.9). It is also possible to interpret the generalized harmonic map given

above as a generalized string model. Although the metric of the base space $M$ is Euclidean, we can apply a Wick rotation $\tau = i\rho$ to obtain a Minkowski-like structure on $M$. Then, $M$ represents the world-sheet of a bosonic string in which $\tau$ is measures the time and $z$ is the parameter along the string. The string is "embedded" in the target space $N$ whose metric is conformally flat and explicitly depends on the time parameter $\tau$. We will see in the next section that this embedding becomes more plausible when the target space is subject to a dimensional extension. In the present example, it is necessary to apply a Wick rotation in order to interpret the base space as a string world-sheet. This is due to the fact that both coordinates $\rho$ and $z$ are spatial coordinates. However, this can be avoided by considering other classes of gravitational fields with timelike Killing vector fields; examples will be given below.

The most studied solutions belonging to the class of stationary axisymmetric fields are the asymptotically flat solutions. Asymptotic flatness imposes conditions on the metric functions which in the cylindrical coordinates used here can be formulated in the form

$$\lim_{x^a\to\infty} f = 1 + O\left(\frac{1}{x^a}\right) \ , \quad \lim_{x^a\to\infty} \omega = c_1 + O\left(\frac{1}{x^a}\right) \ , \quad \lim_{x^a\to\infty} \Omega = O\left(\frac{1}{x^a}\right) \tag{5.3.14}$$

where $c_1$ is an arbitrary real constant which can be set to zero by appropriately choosing the angular coordinate $\varphi$. If we choose the domain of the spatial coordinates as $\rho \in [0, \infty)$ and $z \in (-\infty, +\infty)$, from the asymptotic flatness conditions it follows that the coordinates of the target space $N$ satisfy the boundary conditions

$$\dot{X}^\mu(\rho, -\infty) = 0 = \dot{X}^\mu(\rho, \infty) \ , \quad X'^\mu(\rho, -\infty) = 0 = X'^\mu(\rho, \infty) \tag{5.3.15}$$

where the dot stands for a derivative with respect to $\rho$ and the prime represents derivation with respect to $z$. These relationships are known in string theory (16) as the Dirichlet and Neumann boundary conditions for open strings, respectively, with the extreme points situated at infinity. We thus conclude that if we assume $\rho$ as a "time" parameter for stationary axisymmetric gravitational fields, an asymptotically flat solution corresponds to an open string with endpoints attached to $D-$branes situated at plus and minus infinity in the $z-$direction.

## 5.4 Dimensional extension

In order to further analyze the analogy between gravitational fields and bosonic string models, we perform an arbitrary dimensional extension of the target space $N$, and study the conditions under which this dimensional extension does not affect the field equations of the gravitational field. Consider an $(m \to D)-$generalized harmonic map. As before we denote by $\{x^a\}$ the coordinates on $M$. Let $\{X^\mu, X^\alpha\}$ with $\mu = 1,2$ and $\alpha = 3,4,...,D$ be the coordinates on $N$. The metric structure on $M$ is again $\gamma = \gamma(x)$, whereas the metric on $N$ can in general depend on all coordinates of $M$ and $N$, i.e. $G = G(X^\mu, X^\alpha, x^a)$. The general structure of the corresponding field equations is as given in (5.3.1). They can be divided into one set of equations for $X^\mu$ and one set of equations for $X^\alpha$. According to the results of the last section, the class of gravitational fields under consideration can be represented as a $(2 \to 2)-$generalized harmonic map so that we can assume that the main gravitational variables are contained in the coordinates $X^\mu$ of the target space. Then, the gravitational sector of the target space will be contained in the components $G_{\mu\nu}$ $(\mu, \nu = 1,2)$ of the metric, whereas the components $G_{\alpha\beta}$ $(\alpha, \beta = 3,4,...,D)$ represent the sector of the dimensional extension.

Clearly, the set of differential equations for $X^\mu$ also contains the variables $X^\alpha$ and its derivatives $\partial_a X^\alpha$. For the gravitational field equations to remain unaffected by this dimensional extension we demand the vanishing of all the terms containing $X^\alpha$ and its derivatives in the equations for $X^\mu$. It is easy to show that this can be achieved by imposing the conditions

$$G_{\mu\alpha} = 0\,, \quad \frac{\partial G_{\mu\nu}}{\partial X^\alpha} = 0\,, \quad \frac{\partial G_{\alpha\beta}}{\partial X^\mu} = 0\,. \tag{5.4.1}$$

That is to say that the gravitational sector must remain completely invariant under a dimensional extension, and the additional sector cannot depend on the gravitational variables, i.e., $G_{\alpha\beta} = G_{\alpha\beta}(X^\gamma, x^a)$, $\gamma = 3,4,...,D$. Furthermore, the variables $X^\alpha$ must satisfy the differential equations

$$\frac{1}{\sqrt{|\gamma|}}\partial_b\left(\sqrt{|\gamma|}\gamma^{ab}\partial_a X^\alpha\right) + \Gamma^\alpha_{\beta\gamma}\,\gamma^{ab}\,\partial_a X^\beta \partial_b X^\gamma + G^{\alpha\beta}\gamma^{ab}\,\partial_a X^\gamma\,\partial_b G_{\beta\gamma} = 0\,. \tag{5.4.2}$$

This shows that any given $(2 \to 2)-$generalized map can be extended, without affecting the field equations, to a $(2 \to D)-$generalized harmonic map.

It is worth mentioning that the fact that the target space $N$ becomes split in two separate parts implies that the energy-momentum tensor $T_{ab} = \delta\mathcal{L}/\delta\gamma^{ab}$ separates into one part belonging to the gravitational sector and a second one following from the dimensional extension, i.e. $T_{ab} = T_{ab}(X^\mu, x) + T_{ab}(X^\alpha, x)$. The generalized conservation law as given in (5.3.8) is satisfied by the sum of both parts.

Consider the example of stationary axisymmetric fields given the metrics (5.3.9). Taking into account the conditions (5.4.1), after a dimensional extension the metric of the target space becomes

$$G = \begin{pmatrix} \frac{\rho}{2f^2} & 0 & 0 & \cdots & 0 \\ 0 & \frac{\rho}{2f^2} & 0 & \cdots & 0 \\ 0 & 0 & G_{33}(X^\alpha, x) & \cdots & G_{3D}(X^\alpha, x) \\ . & . & \cdots & \cdots & \cdots \\ 0 & 0 & G_{D3}(X^\alpha, x) & \cdots & G_{DD}(X^\alpha, x) \end{pmatrix} . \tag{5.4.3}$$

Clearly, to avoid that this metric becomes degenerate we must demand that $\det(G_{\alpha\beta}) \neq 0$, a condition that can be satisfied in view of the arbitrariness of the components of the metric. With the extended metric, the Lagrangian density gets an additional term

$$\begin{aligned} \mathcal{L} = \quad & \frac{\rho}{2f^2}\left[(\partial_\rho f)^2 + (\partial_z f)^2 + (\partial_\rho \Omega)^2 + (\partial_z \Omega)^2\right] \\ & + \left(\partial_\rho X^\alpha \partial_\rho X^\beta + \partial_z X^\alpha \partial_z X^\beta\right) G_{\alpha\beta} \,, \end{aligned} \tag{5.4.4}$$

which nevertheless does not affect the field equations for the gravitational variables $f$ and $\Omega$. On the other hand, the new fields must be solutions of the extra field equations

$$\left(\partial_\rho^2 + \partial_z^2\right) X^\alpha + \Gamma^\alpha{}_{\beta\gamma}\left(\partial_\rho X^\beta \partial_\rho X^\gamma + \partial_z X^\beta \partial_z X^\gamma\right) \tag{5.4.5}$$

$$+ G^{\alpha\gamma}\left(\partial_\rho X^\beta \partial_\rho G_{\beta\gamma} + \partial_z X^\beta \partial_z G_{\beta\gamma}\right) = 0 \,. \tag{5.4.6}$$

An interesting special case of the dimensional extension is the one in which the extended sector is Minkowskian, i.e. for the choice $G_{\alpha\beta} = \eta_{\alpha\beta}$ with additional fields $X^\alpha$ given as arbitrary harmonic functions. This choice opens the possibility of introducing a "time" coordinate as one of the additional dimen-

sions, an issue that could be helpful when dealing with the interpretation of gravitational fields in this new representation.

The dimensional extension finds an interesting application in the case of static axisymmetric gravitational fields. As mentioned in Section 4.1, these fields are obtained from the general stationary fields in the limiting case $\Omega = 0$ (or equivalently, $\omega = 0$). If we consider the representation as an $SL(2,R)/SO(2)$ nonlinear sigma model or as a $(2 \to 2)-$generalized harmonic map, we see immediately that the limit $\Omega = 0$ is not allowed because the target space becomes 1-dimensional and the underlying metric is undefined. To avoid this degeneracy, we first apply a dimensional extension and only then calculate the limiting case $\Omega = 0$. In the most simple case of an extension with $G_{\alpha\beta} = \delta_{\alpha\beta}$, the resulting $(2 \to 2)-$generalized map is described by the metrics $\gamma_{ab} = \delta_{ab}$ and

$$G = \begin{pmatrix} \frac{\rho}{2f^2} & 0 \\ 0 & 1 \end{pmatrix} \tag{5.4.7}$$

where the additional dimension is coordinatized by an arbitrary harmonic function which does not affect the field equations of the only remaining gravitational variable $f$. This scheme represents an alternative method for exploring static fields on nondegenerate target spaces. Clearly, this scheme can be applied to the case of gravitational fields possessing two hypersurface orthogonal Killing vector fields.

Our results show that a stationary axisymmetric field can be represented as a string "living" in a $D$-dimensional target space $N$. The string world-sheet is parametrized by the coordinates $\rho$ and $z$. The gravitational sector of the target space depends explicitly on the metric functions $f$ and $\Omega$ and on the parameter $\rho$ of the string world-sheet. The sector corresponding to the dimensional extension can be chosen as a $(D-2)-$dimensional Minkowski spacetime with time parameter $\tau$. Then, the string world-sheet is a 2-dimensional flat hypersurface which is "frozen" along the time $\tau$.

## 5.5 The general solution

If we take as seed metric the general static solution, the application of two HXK transformations generates a stationary solution with an infinite number of gravitoelectric and gravitomagnetic multipole moments. The HKX method is applied at the level of the Ernst potential from which the metric functions

can be calculated by using the definition of the Ernst potential $E$ and the field equations for $\gamma$. The resulting expressions in the general case are quite cumbersome. We quote here only the special case in which only an arbitrary quadrupole parameter is present. In this case, the result can be written as

$$\begin{aligned} f &= \frac{R}{L} e^{-2qP_2Q_2} , \\ \omega &= -2a - 2\sigma \frac{\mathcal{M}}{R} e^{2qP_2Q_2} , \\ e^{2\gamma} &= \frac{1}{4}\left(1 + \frac{M}{\sigma}\right)^2 \frac{R}{x^2 - y^2} e^{2\hat{\gamma}} , \end{aligned} \tag{5.5.1}$$

where

$$\begin{aligned} R &= a_+ a_- + b_+ b_- , \qquad L = a_+^2 + b_+^2 , \\ \mathcal{M} &= \alpha x(1-y^2)(e^{2q\delta_+} + e^{2q\delta_-})a_+ + y(x^2-1)(1 - \alpha^2 e^{2q(\delta_+ + \delta_-)})b_+ , \\ \hat{\gamma} &= \frac{1}{2}(1+q)^2 \ln\frac{x^2-1}{x^2-y^2} + 2q(1-P_2)Q_1 + q^2(1-P_2)\Big[(1+P_2)(Q_1^2 - Q_2^2) \\ &\quad + \frac{1}{2}(x^2-1)(2Q_2^2 - 3xQ_1Q_2 + 3Q_0Q_2 - Q_2')\Big] . \end{aligned} \tag{5.5.2}$$

Here $P_l(y)$ and $Q_l(x)$ are Legendre polynomials of the first and second kind respectively. Furthermore

$$\begin{aligned} a_\pm &= x(1 - \alpha^2 e^{2q(\delta_+ + \delta_-)}) \pm (1 + \alpha^2 e^{2q(\delta_+ + \delta_-)}) , \\ b_\pm &= \alpha y(e^{2q\delta_+} + e^{2q\delta_-}) \mp \alpha(e^{2q\delta_+} - e^{2q\delta_-}) , \\ \delta_\pm &= \frac{1}{2}\ln\frac{(x \pm y)^2}{x^2-1} + \frac{3}{2}(1 - y^2 \mp xy) + \frac{3}{4}[x(1-y^2) \mp y(x^2-1)]\ln\frac{x-1}{x+1} , \end{aligned}$$

the quantity $\alpha$ being a constant

$$\alpha = \frac{\sigma - M}{a} , \qquad \sigma = \sqrt{M^2 - a^2} . \tag{5.5.3}$$

The physical significance of the parameters entering this metric can be clarified by calculating the Geroch-Hansen (18; 19) multipole moments

$$M_{2k+1} = J_{2k} = 0 , \quad k = 0, 1, 2, ... \tag{5.5.4}$$

$$M_0 = M\,, \quad M_2 = -Ma^2 + \frac{2}{15}qM^3\left(1 - \frac{a^2}{M^2}\right)^{3/2}\,, \ldots \tag{5.5.5}$$

$$J_1 = Ma\,, \quad J_3 = -Ma^3 + \frac{4}{15}qM^3a\left(1 - \frac{a^2}{M^2}\right)^{3/2}\,, \ldots. \tag{5.5.6}$$

The vanishing of the odd gravitoelectric ($M_n$) and even gravitomagnetic ($J_n$) multipole moments is a consequence of the symmetry with respect to the equatorial plane. From the above expressions we see that $M$ is the total mass of the body, $a$ represents the specific angular momentum, and $q$ is related to the deviation from spherical symmetry. All higher multipole moments can be shown to depend only on the parameters $M$, $a$, and $q$.

We analyzed the geometric and physical properties of the above solution. The special cases contained in the general solution suggest that it can be used to describe the exterior asymptotically flat gravitational field of rotating body with arbitrary quadrupole moment. This is confirmed by the analysis of the motion of particles on the equatorial plane. The quadrupole moment turns out to drastically change the geometric structure of spacetime as well as the motion of particles, especially near the gravitational source.

We investigated in detail the properties of the Quevedo-Mashhoon (QM) spacetime which is a generalization of Kerr spacetime, including an arbitrary quadrupole. Our results show (20) that a deviation from spherical symmetry, corresponding to a non-zero electric quadrupole, completely changes the structure of spacetime. A similar behavior has been found in the case of the Erez-Rosen spacetime. In fact, a naked singularity appears that affects the ergosphere and introduces regions where closed timelike curves are allowed. Whereas in the Kerr spacetime the ergosphere corresponds to the boundary of a simply-connected region of spacetime, in the present case the ergosphere is distorted by the presence of the quadrupole and can even become transformed into non simply-connected regions. All these changes occur near the naked singularity which is situated at $x = 1$, a value that corresponds to the radial distance $r = M + \sqrt{M^2 - a^2}$ in Boyer-Lindquist coordinates. In the limiting case $a/M > 1$, the multipole moments and the metric become complex, indicating that the physical description breaks down. Consequently, the extreme Kerr black hole represents the limit of applicability of the QM spacetime.

Since standard astrophysical objects satisfy the condition $a/M < 1$, we can conclude that the QM metric can be used to describe their exterior grav-

itational field. Two alternative situations are possible. If the characteristic radius of the body is greater than the critical distance $M + \sqrt{M^2 - a^2}$, i.e. $x > 1$, the exterior solution must be matched with an interior solution in order to describe the entire spacetime. If, however, the characteristic radius of the body is smaller than the critical distance $M + \sqrt{M^2 - a^2}$, the QM metric describes the field of a naked singularity.

# 6 Accretion disks in the Hartle-Thorne spacetime

The influx of gas and dust or, more general, diffuse material, towards a central gravitating object is dubbed *accretion*, mostly occurring through the formation of *accretion disks* (22; 23; 24). The formation of an accretion disk is unquestionably one of the most prevalent processes in relativistic astrophysics and, importantly, it yields significant observational manifestations. Notably, the accretion of matter onto relativistic objects, such as black holes and neutron stars, stands out as one of the most efficient mechanisms for energy release in the field of astrophysics (25). Undoubtedly, the most remarkable observational manifestation is the accretion onto a black hole that results in the release of an enormous amount of energy per unit of accreted mass and showcases the dynamics associated with black hole accretion.

Accretion disks enable the observation of the radiation emitted by matter in rotational motion around a compact object. By analyzing the emitted spectra of the disk, valuable information about the nature of the central object undergoing accretion can be obtained. These observations provide insights into the properties and characteristics of the accreting central object, contributing to our understanding of astrophysical phenomena.

The exploration of central compact objects, which also includes supermassive central objects, carries immense importance in contemporary astrophysics. The origin of these objects is still a topic of ongoing discussion. Comprehending their physical attributes necessitates indirect research methods, such as examining *accretion disks*. Accretion disks play a crucial role in uncovering the fundamental properties of the aforementioned structures. By conducting thorough analyses and observations of accretion disks, we can acquire valuable knowledge about the development and dynamics of central compact objects[1].

[1]Nevertheless, the incoming observations can also shed some new light on possible deviations from general relativity in the incoming years. Consequently, the possible existence

Accretion disk luminosity for compact objects can be modeled using various solutions to Einstein's field equations. This includes the gravitational field of neutral black holes, as described in Ref. (26), or the outside field of white dwarfs and neutron stars, as discussed in Refs. (24; 27; 28; 29). Additionally, exotic objects such as boson stars (30; 31; 32; 33) or gravastars (34) can also be considered. Observations related to accretion disks provide valuable insights into these objects as well. Examples include the motion of stars near the galactic center (35; 36; 37), the spectra of X-ray binary systems (38) and the emission by the accretion disks of binary black holes (39; 40). Other examples encompass the shadow of supermassive black hole candidates in the nucleus of the M87 galaxy (41), among others. It is worth noting that certain features of the accretion disk depend on the underlying space-time geometry (42). Hence, observations of accretion disks can be utilized to impose constraints on the geometry, as discussed in (43). By comparing theoretical models with observational data, we can gain insights into the nature of compact objects and the properties of the space-time in their vicinity.

Among all possible spacetimes modeling compact objects, from which we can infer accretion disk properties, the Hartle-Thorne metric represents a useful tool for describing the geometry around slowly rotating and slightly deformed objects in strong gravitational fields. As stated, it provides a framework for studying real astrophysical objects ranging from celestial bodies like planets to neutron stars. The metric is characterized by three multipole moments: the total mass, the angular and quadrupole momenta. These parameters describe several astrophysical phenomena (44; 45; 46; 47).

One notable advantage of the Hartle-Thorne metric is its flexibility. In cases where angular momentum is absent, it characterizes a naked singularity. However, by incorporating angular momentum and expressing the quadrupole moment based on it, the metric transforms into the well-known Kerr metric. When linear terms in angular momentum are present without the quadrupole moment, it corresponds to the Lense-Thirring solution. Additionally, in the absence of angular momentum, a comparison can be made between the Hartle-Thorne metric and the approximate Erez-Rosen solution (48). Consequently, the Hartle-Thorne solution serves as a valuable reference point for modeling intricate variations of central compact objects.

In this work, we construct a theoretical scheme to determine the accre-

of exotic compact objects cannot be ignored, as most observations of black hole candidates do not allow one to study the geometry near such astrophysical sources yet.

tion disk, following the standard theory of black hole accretion developed in (49; 50), which can be adapted to the Hartle-Thorne solution within the context of Einstein's equations. So, we first compute the particle motion in such a metric, emphasizing the role of the aforementioned three free parameters. Afterwards, we determine the circular orbits, the innermost stable circular orbits (ISCOs) and the kinematic properties of the metric, used to infer the spectral properties of thin accretion disks. We compare our findings with those of the Schwarzschild and Kerr metrics as limiting cases of the Hartle-Thorne spacetime. We motivate this, noticing that specific properties of given compact objects can modify the form of the metric and so, utilizing the Hartle-Thorne metric, one can compute the luminosity and fluxes associated with these central compact objects. These calculations provide valuable insights into the observable properties of accretion processes and the radiative emissions from the surrounding matter. Finally, theoretical interpretations of our outcomes are critically discussed, employing generic neutron star models that are compared with our framework.

The difference between the current work and the above-mentioned and other works lies, firstly, in different metrics, which are used for different purposes. For example, in our previous works (51; 52; 53) we examined the motion of test particles in the gravitational field of a Schwarzschild black hole surrounded by spherically distributed dark matter, possessing non-zero isotropic, anisotropic, and tangential pressures. These studies indicate that the inclusion of dark matter pressure significantly alters the geometry around the Schwarzschild black hole, impacting the radiative flux, differential luminosity, and spectral luminosity of the accretion disk. In this paper, we study the geometry around astrophysical objects such as neutron stars, whose interior and exterior geometry is well described by the Hartle–Thorne solution.

In Sect. 6.1, we review the Hartle-Thorne metric and compare it with other known solutions, In Sect. 6.2, we consider the circular orbits and basic parameters of neutral test particles in the Hartle-Thorne spacetime. In Sect. 6.3, we review the Novikov-Page-Thorne model and present our numerical results for the spectral properties of the accretion disks. In Sect. 6.4, we discuss about neutron star physics. Finally, in Sect. 6.5, we present the conclusions and perspectives of our work. Throughout the paper we make use of geometrized units setting $G = c = 1$. This work was published in (21).

## 6.1 Particle motion in the Hartle-Thorne metric

The line element for the Hartle-Thorne metric is (54)

$$
\begin{aligned}
ds^2 = &-\left(1-\frac{2M}{r}\right)\left[1+2k_1P_2(\cos\theta)+2\left(1-\frac{2M}{r}\right)^{-1}\frac{J^2}{r^4}(2\cos^2\theta-1)\right]dt^2\\
&+\left(1-\frac{2M}{r}\right)^{-1}\left[1-2k_2P_2(\cos\theta)-2\left(1-\frac{2M}{r}\right)^{-1}\frac{J^2}{r^4}\right]dr^2\\
&+r^2[1-2k_3P_2(\cos\theta)](d\theta^2+\sin^2\theta d\phi^2)-\frac{4J}{r}\sin^2\theta dt d\phi
\end{aligned}
\tag{6.1.1}
$$

with

$$
\begin{aligned}
k_1 &= \frac{J^2}{Mr^3}\left(1+\frac{M}{r}\right)+\frac{5}{8}\frac{Q-J^2/M}{M^3}Q_2^2\left(\frac{r}{M}-1\right), \quad k_2 = k_1-\frac{6J^2}{r^4},\\
k_3 &= k_1+\frac{J^2}{r^4}+\frac{5}{4}\frac{Q-J^2/M}{M^2\left(r^2-2Mr\right)^{1/2}}Q_2^1\left(\frac{r}{M}-1\right),
\end{aligned}
$$

and

$$
P_2(\cos\theta)=\frac{1}{2}(3\cos^2\theta-1),\;\; Q_2^1(x)=(x^2-1)^{1/2}\left[\frac{3x}{2}\ln\frac{x+1}{x-1}-\frac{3x^2-2}{x^2-1}\right],
$$

$$
Q_2^2(x)=(x^2-1)\left[\frac{3}{2}\ln\frac{x+1}{x-1}-\frac{3x^3-5x}{(x^2-1)^2}\right],
$$

where $x = r/M-1$, $P_2(x)$ is the second Legendre polynomial of the first kind, $Q_l^m$ are the associated Legendre polynomials of the second kind and the constants $M$, $J$ and $Q$ are, as mentioned earlier, the total mass, angular momentum and mass quadrupole moment of a rotating star, respectively. In addition, $J \sim \Omega_{Star}$ and $Q \sim \Omega_{Star}^2$, where $\Omega_{Star}$ is the angular velocity of the central object, or a star, behaving as the source of gravity.

In general, the Hartle-Thorne metric encompasses both interior and exterior solutions that describe the gravitational field within and outside a compact object, respectively. However, when one investigates the accretion disk, focusing on the exterior case appears sufficient. Indeed, this occurs because the accretion disk is primarily influenced by the gravitational field outside

the compact object. However, there are certain situations where it becomes necessary to explore the interior gravitational field of a compact object as well as the exterior one. This is particularly relevant when constructing quantities such as mass-radius relations or mass-central density profiles. In such cases, it is important to appropriately consider both the interior and exterior solutions of the Hartle-Thorne metric in order to obtain a complete description of the compact object.

### 6.1.1 Comparison with alternative spacetimes

Here we review the relationship of the Hartle-Thorne metric with other solutions in the literature, survey studies on accretion disks in those spacetimes and highlight some open issues in this direction.

The exterior Hartle-Thorne solution characterizes the geometry surrounding compact objects with slow rotation and slight deformations. In their groundbreaking paper (55), Hartle and Thorne initially attempted to compare this solution with the well-known Kerr solution. It has been demonstrated that by selecting a specific value for the quadrupole moment, denoted as $q = j^2$, and applying intricate coordinate transformations, the Hartle-Thorne solution converges to the approximate Kerr solution in the case of slow rotation. This implies that the applicability of the Kerr solution is limited and it can only describe a particular category of objects, namely the geometry around rotating black holes[2].

Subsequently, the Hartle-Thorne metric can be compared with a static spacetime describing the geometry around deformed objects, in particular, with the Erez-Rosen metric[3] (56). Then, by using the Geroch-Hansen invariant definition of multipole moments (57; 58) it was established that the monopole moment corresponds to the total mass, the dipole moment is the angular momentum, and the quadrupole moment contains an intrinsic part, due to the deformation of the source, and a second term due to rotation. As a

[2]The luminosity of the accretion disk in the Kerr spacetime has been extensively investigated in the scientific literature.

[3]It was shown that the static Hartle-Thorne solution with $j = 0$ reduces to the approximate Erez-Rosen solution in the limiting case of a small deformation (48). However, before finding the coordinate transformations to establish the relationship between the parameters of the solutions, it was necessary to generalize the Erez-Rosen metric by applying a Zipoy-Voorhees transformation, which introduces a new parameter that must be fixed in order to obtain the required transformations (48).

result, it was shown that the Hartle-Thorne parameters $M$ and $Q$ are related to those of the Erez-Rosen metric as follows $M = M_{ER}(1 - q_{ER})$ and $Q = -(4/5)q_{ER}M_{ER}^3$. This result allows one to find unambiguously the coordinate transformations between the static Hartle-Thorne and the approximate Erez-Rosen solutions[4].

A further attempt to find the relationship between the Hartle-Thorne and Erez-Rosen solutions was made by Frutos-Alfaro and Soffel in the limit of $\sim M^2$ and $\sim Q^2$ (60). To this end, the original exterior Hartle-Thorne solution was generalized to include new terms $\sim Q^2$ for a non-rotating case. The advantage of this approach is that it is not necessary to perform a Zipoy-Voorhees transformation in order to obtain the corresponding coordinate transformations, which turned out to have a completely different form. It was concluded that the approximation determines the coordinate transformation (for more details see e.g. Ref. (61)). To the knowledge of the authors, the luminosity of accretion disks in the Erez-Rosen spacetime has not been studied yet in the literature.

Additionally, in Refs. (62; 63; 64; 65; 66), it was found a whole new class of exterior exact solutions with an infinite number of parameters, containing not only the mass, rotation parameter, and quadrupole parameter, but also the Zipoy-Voorhees parameter, charge, and the Taub-NUT parameter, among others[5]. In this respect, one of the main drawbacks of the exterior exact solutions is the fact that it is hard or sometimes even impossible to find their interior counterparts. Nonetheless, as above stated, for most of the astrophysical phenomena the exterior exact solutions are more than sufficient and play a pivotal and occasionally ultimate role. The luminosity of the accretion disk in the spacetime combining both Kerr and Erez-Rosen solutions has not been studied yet.

In the weak field regime, namely in the post-Newtonian approximation, it was shown that the Hartle-Thorne solution reduces to the Fock solution with quadrupole moment (67). The generalization of the Hartle-Thorne solution to quartic order in angular velocity has been obtained in Ref. (68). Undoubtedly, the extension of the Hartle-Thorne solution may have a wider application in

[4]Some details about the Zipoy-Voorhees transformations that are necessary to compare the Erez-Rosen and Hartle-Thorne solutions can be found in Ref. (59).

[5]This solution contains as a specific case the solution combining both Erez Rosen and Kerr solutions. Using the prescriptions provided in Refs. (55; 48), it was demonstrated that this particular Quevedo-Mashhoon solution in the limiting case of slow rotation and small deformation was equivalent to the Hartle-Thorne solution (54).

astrophysics[6].

In view of recent developments (70), it should also be possible to establish the relationship between the Hartle-Thorne solution and $q$-metric[7] and its extension that includes the rotation parameter (71; 72). However, this issue is out of the scope of the present work and possibly will be addressed in future studies.

Given the remarkable properties of the Hartle-Thorne spacetime and its widespread applications, it is highly intriguing to explore its implications in the context of accretion disks. By incorporating quadrupole terms and considering modifications to the standard Zipoy-Voorhees metric, we can account for additional factors such as mass and other properties that may influence the dynamics of the system. This allows us to extend the applicability of the Hartle-Thorne solution beyond static spherically symmetric configurations and incorporate rotation effects. Remarkably, the predictions derived from our analysis are anticipated to be tested experimentally in the near future, further validating the significance of our findings. In this respect, below we elucidate the main features of the Hartle-Thorne solution in view of observable signatures that can be obtained from it.

## 6.2 Circular orbits in the Hartle-Thorne space-time

We focus our analysis on the equatorial plane, where the polar angle $\theta$ is fixed at $\pi/2$. Within this restricted region, we investigate the motion of neutral test particles that follow circular orbits. By employing the well-established Euler-Lagrange formalism, we are able to determine various orbital parameters for these particles, including the angular velocity, angular momentum, and energy[8]. These quantities play a crucial role in characterizing the dynamics of the test particles and provide valuable insights into their behavior within the considered gravitational field.

[6] Additionally, it was shown that the so-called Sedrakyan-Chubaryan solution is equivalent to the the Hartle-Thorne solution (69).

[7] Sometimes, this metric is known in the literature as the Zipoy-Voorhees metric, $\delta$-metric and $\gamma$-metric.

[8] The formulas for the angular velocity $\Omega$, angular momentum $L$, and energy $E$ in the Hartle-Thorne spacetime were initially derived in Ref. (73). However, it is important to exercise caution when referring to (73) due to the presence of certain typographical errors.

### 6.2.1 Angular momentum and energy

The angular velocity for corotating/counterrotating particles on circular orbits for a generic stationary axisymmetric metric (74) is given by

$$\Omega = \frac{d\phi}{dt} = \frac{-\partial_r g_{t\phi} \pm \sqrt{(\partial_r g_{t\phi})^2 - (\partial_r g_{tt})(\partial_r g_{\phi\phi})}}{\partial_r g_{\phi\phi}}, \tag{6.2.1}$$

and for the Hartle-Thorne spacetime it acquires the form

$$\Omega = \Omega_0 \left[1 \mp j W_1(r) + j^2 W_2(r) + q W_3(r)\right], \tag{6.2.2}$$

where $j = J/M^2$, $q = Q/M^3$, $\Omega_0$ is the angular velocity for the Schwarzschild metric, and $W_{1;2;3}$ are reported below

$$\begin{aligned}
\Omega_0(r) &= \frac{M^{1/2}}{r^{3/2}}, && (6.2.3)\\
W_1(r) &= \frac{M^{3/2}}{r^{3/2}}, && (6.2.4)\\
W_2(r) &= \left[16M^2r^4(r-2M)\right]^{-1}\left(48M^7 - 80M^6 r + 4M^5 r^2\right. \\
&- \left. 18M^4 r^3 + 40M^3 r^4 + 10M^2 r^5 + 15Mr^6 - 15r^7\right) + W(r), && (6.2.5)\\
W_3(r) &= 5\left[16M^2 r(r-2M)\right]^{-1} \\
&\times \left(6M^4 - 8M^3 r - 2M^2 r^2 - 3Mr^3 + 3r^4\right) - W(r), && (6.2.6)\\
W(r) &= \frac{15(r^3 - 2M^3)}{32M^3} \ln\left(\frac{r}{r-2M}\right). && (6.2.7)
\end{aligned}$$

Given the generic orbital angular momentum,

$$L = \frac{g_{t\phi} + \Omega g_{\phi\phi}}{\sqrt{-g_{tt} - 2\Omega g_{t\phi} - \Omega^2 g_{\phi\phi}}}, \tag{6.2.8}$$

we compute it for the Hartle-Thorne metric, having

$$L = L_0 \left[1 \mp jH_1(r) + j^2 H_2(r) + qH_3(r)\right], \tag{6.2.9}$$

where, analogously to the above case, $L_0$, say the angular momentum for the Schwarzschild metric and the supporting functions $H_{1;2;3}$ are reported below

$$\begin{aligned}
L_0(r) &= r\sqrt{\frac{M}{r-3M}}, && (6.2.10)\\
H_1(r) &= \frac{3M^{3/2}(r-2M)}{r^{3/2}(3M-r)}, && (6.2.11)\\
H_2(r) &= \left[16M^2r^4(r-3M)^2\right]^{-1} \\
&\times \left[144M^8 - 144M^7r + 20M^6r^2 - 98M^5r^3 + 147M^4r^4\right. \\
&+ \left. 205M^3r^5 - 260M^2r^6 + 105Mr^7 - 15r^8\right] + H(r), && (6.2.12)\\
H_3(r) &= 5\left[16M^2r(3M-r)\right]^{-1} \\
&\times \left(6M^4 - 7M^3r - 16M^2r^2 + 12Mr^3 - 3r^4\right) - H(r), && (6.2.13)\\
H(r) &= 15\left[32M^3(3M-r)\right]^{-1} \\
&\times \left(6M^4 + 2M^3r - 9M^2r^2 + 5Mr^3 - r^4\right)\ln\left(\frac{r}{r-2M}\right) && (6.2.14)
\end{aligned}$$

Afterwards, the generic expression for the energy of test particles on circular orbit,

$$E = -\frac{g_{tt} + \Omega g_{t\phi}}{\sqrt{-g_{tt} - 2\Omega g_{t\phi} - \Omega^2 g_{\phi\phi}}}, \tag{6.2.15}$$

leads to

$$E = E_0\left[1 \mp jF_1(r) + j^2F_2(r) + qF_3(r)\right], \tag{6.2.16}$$

for the Hartle-Thorne spacetime. Here, $E_0$ is the energy for the Schwarzschild

space-time and the supporting functions, $F_{1;2;3}$, are

$$E_0(r) = \frac{r-2M}{\sqrt{r(r-3M)}}, \tag{6.2.17}$$

$$F_1(r) = \frac{M^{5/2}r^{-1/2}}{(r-2M)(r-3M)}, \tag{6.2.18}$$

$$\begin{aligned} F_2(r) &= \left[16Mr^4(2M-r)(r-3M)^2\right]^{-1} \\ &\times \Big(-144M^8+144M^7r+28M^6r^2+58M^5r^3+176M^4r^4 \\ &- 685M^3r^5+610M^2r^6-225Mr^7+30r^8\Big) - F(r), \end{aligned} \tag{6.2.19}$$

$$\begin{aligned} F_3(r) &= -5\left[16Mr(r-2M)(r-3M)\right]^{-1} \\ &\times \left(6M^4+14M^3r-41M^2r^2+27Mr^3-6r^4\right) + F(r), \end{aligned} \tag{6.2.20}$$

$$F(r) = \frac{15r(8M^2-7Mr+2r^2)}{32M^2(3M-r)} \ln\left(\frac{r}{r-2M}\right). \tag{6.2.21}$$

As mentioned in the previous section, these quantities reduce to the corresponding Schwarzschild values for $q \to 0$ and $j \to 0$.

The novelty of our work lies in the fact that all analytic expressions, describing test particles in circular orbits, were applied to the description of accretion disks. We explicitly showed that, in the Hartle–Thorne metric the parameters of the source such as total mass, angular momentum and quadrupole momentum affect the motion of test particles and the whole structure of accretion disks. In other spacetimes these parameters appear as well, however in most of the cases those spacetimes are used for other goals.

In the past related works usually black hole and naked singularity solutions have been exploited to analyze accretion disks within the Novikov–Thorne–Page model. Moreover, Bambi and Barausse (75), considered a solution describing the geometry around compact objects and used it to constraint the quadrupole moment of the source exploiting X-ray data of the thermal spectrum of black hole candidates' accretion disk. Accordingly, the results in this work are different.

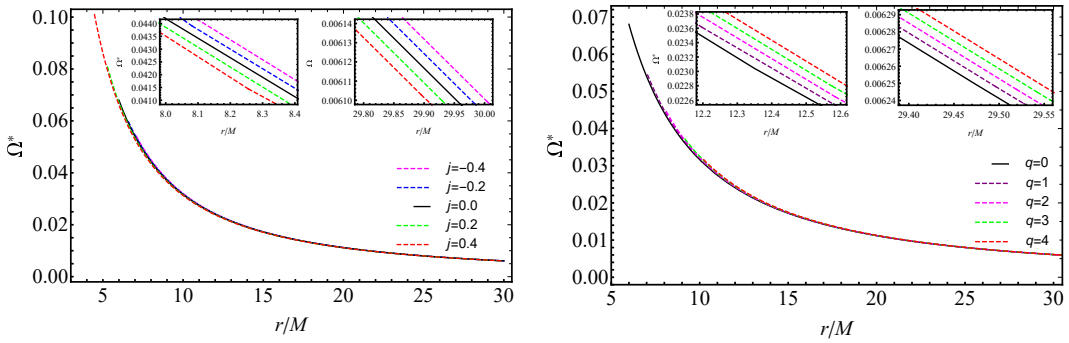


**Figure 6.1:** Dimensionless angular velocity $\Omega^* = M\Omega$ of test particles versus radial distance $r$ normalized by the total mass $M$ in the Hartle-Thorne space-time. All curves start from $R_{ISCO}$. Left panel: the quadrupole parameter is set as $q = 0$ in all curves. Right panel: the spin parameter is set as $j = 0$ in all curves.

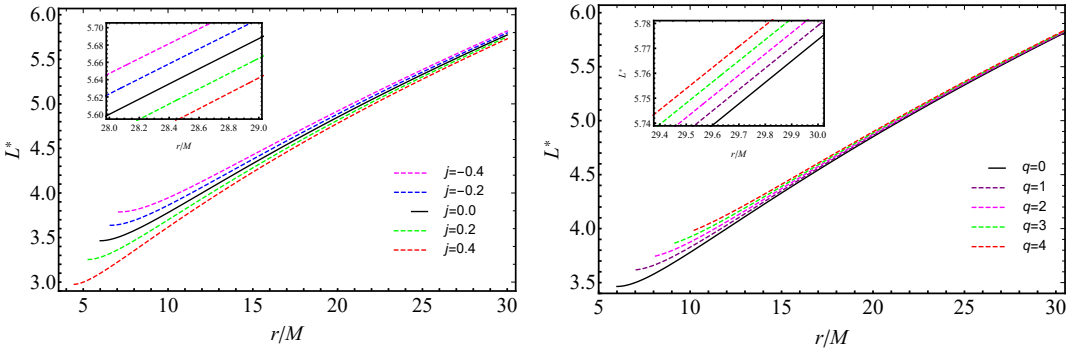


**Figure 6.2:** Angular momentum $L^* = L/M$ of test particles versus radial distance $r$ normalized by the total mass $M$ in the Hartle-Thorne metric. All curves start from $R_{ISCO}$. Left panel: $L^*$ for fixed $q = 0$ and arbitrary $j$. Right panel: for fixed $j = 0$ and arbitrary $q$.

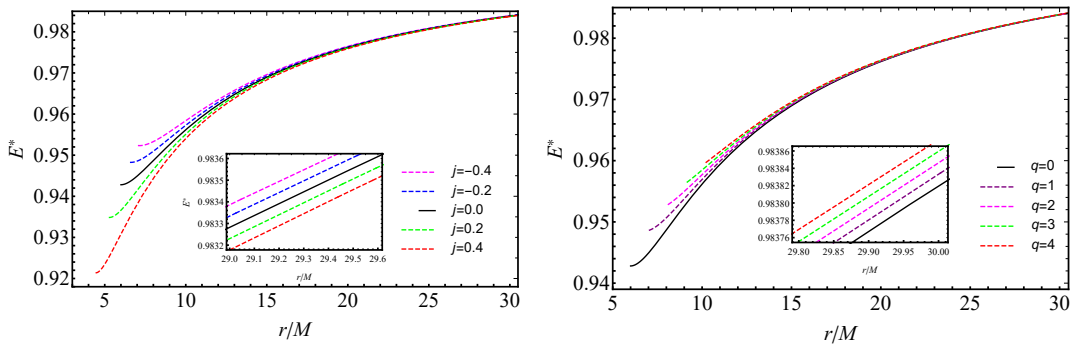


**Figure 6.3:** Energy $E^* = E$ of test particles versus radial distance $r$ normalized by total mass $M$ in the Hartle-Thorne spacetime. All curves start from $R_{ISCO}$. Left panel: $E^*$ for fixed $q = 0$ and arbitrary $j$. Right panel: $E^*$ for fixed $j = 0$ and arbitrary $q$.

### 6.2.2 The innermost stable circular orbits

As we claimed in the introduction, ISCO is the smallest circular orbit around a massive object that can be obtained within the contexts of metric theories. Computing this quantity is manifestly relevant since, there, a test particle can maintain a stable orbit, and so the ISCO radius is function of the mass and angular momentum of the central object determining the accretor. Consequently, in the context of black hole accretion disks, the ISCO is of utmost importance as it represents the inner boundary of the disk itself. Thus, the ISCO radius, dubbed $R_{ISCO}$, is defined via the condition $dL/dr = 0$ or $dE/dr = 0$ (76) and is given by

$$\begin{aligned} R_{ISCO} &= 6M\left[1 \mp \tfrac{2}{3}\sqrt{\tfrac{2}{3}}j + \left(\tfrac{251647}{2592} - 240\ln\tfrac{3}{2}\right)j^2 \right. \\ &\qquad \left. + \left(-\tfrac{9325}{96} + 240\ln\tfrac{3}{2}\right)q\right] \\ &\approx 6M[1 \mp 0.5443j - 0.2256j^2 + 0.1762q]\,. \end{aligned} \tag{6.2.22}$$

Here, the sign in front of $j$ in the expression for the ISCO radius determines the rotation direction of the central object. For co-rotating or prograde orbits, a negative sign is used, while for counter-rotating or retrograde orbits, a positive sign is used. It is worth noting that in the limit of zero angular momentum and quadrupole moment, the ISCO radius reduces to $R^0_{\rm ISCO} = 6M$ for the Schwarzschild spacetime.

It should be mentioned that the analytic formulas for the orbital parameters of test particles such as angular velocity, energy, angular momentum, radius of ISCOs, have been well-known long before this work. However, here we present their corrected analytical expressions and show their graphical representation and practical application to accretion disks.

In addition, one of the key quantities which is of great interest is the *efficiency of converting matter into radiation* (see for details page 662 of Ref. (23))

$$\eta = [1 - E(R_{ISCO})] \times 100\%, \tag{6.2.23}$$

where the energy of test particles $E$ is calculated at $R_{ISCO}$.

### 6.2.3 Numerical analysis of angular velocity, angular momentum and energy of test particles

Here, we report an overall analysis of our numerical findings concerning the angular velocity, angular momentum, the energy of test particles in circular orbits, and all the kinematic quantities of our metric, which are useful for the study of the accretion disk.

Specifically, in Fig. 6.1, we present the orbital angular velocity $\Omega^*(r) = M\Omega$ of test particles as a function of the normalized radial coordinate $r/M$ in the Hartle-Thorne metric. In the left panel, we consider a fixed $q = 0$ and arbitrary $j$, while in the right panel, we fix $j = 0$ and vary $q$. In the left panel, the curves with $j > 0$ are similar to the co-rotating orbits in the Kerr metric or the $q$-metric with $q > 0$, we observe that the angular velocity curves lie below the curve corresponding to the Schwarzschild metric. Instead the curves with $j < 0$ correspond to the counter-rotating orbits in the Kerr spacetime and lie above the curve corresponding to the Schwarzschild metric. In the right panel, which resembles the counter-rotating orbits in the Kerr metric, we see that the angular velocity curves are above the curve obtained in the Schwarzschild solution. It is important to note that in the Hartle-Thorne spacetime, $q > 0$ corresponds to oblate astrophysical objects, while $q < 0$ corresponds to prolate objects. Since most rotating objects are oblate, we focus on cases where $q > 0$ throughout this paper. Furthermore, the limit $q = 0$ describes rotating objects without deformation, distinct from the Kerr spacetime, although many features are similar to the Kerr metric. On the other hand, the limit $j = 0$ represents static deformed objects.

In Fig. 6.2, we present the dimensionless orbital angular momentum $L^*(r) =$

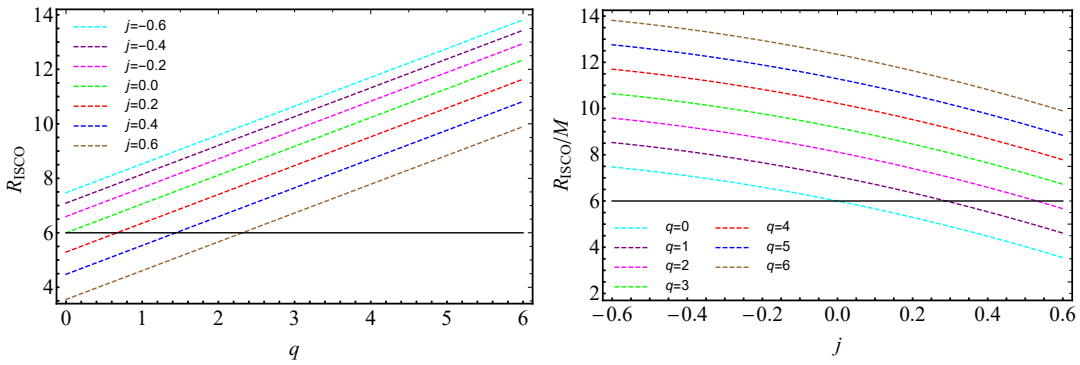


**Figure 6.4:** $R_{ISCO}$ in the Hartle-Thorne spacetime. Left panel: $R_{ISCO}$ versus $q$ for different values of $j$. Right panel: $R_{ISCO}$ versus $j$ for different values of $q$.

$L/M$ of test particles as a function of the normalized radial coordinate $r/M$ in the Hartle-Thorne metric. The left panel corresponds to fixed $q = 0$ and arbitrary $j$, while the right panel represents fixed $j = 0$ and arbitrary $q$. In the left panel, it can be observed that the curves of $L^*$ for $j > 0$ ($j < 0$) lie below (above) with respect to the Schwarzschild case. Moreover, the overall behavior of $L^*$ resembles that of co-rotating (counter-rotating) test particles' orbits in the Kerr spacetime. On the right panel, the Schwarzschild case exhibits smaller values of $L^*$, and the general trend of the curves is similar to the ones observed in the Kerr metric for counter-rotating orbits or the $q$-metric with $q > 0$ cases (see (77) for more detailed information).

In Fig. 6.3, we depict the energy per unit mass $E^* = E$ of test particles as a function of the normalized radial coordinate $r/M$ in the Hartle-Thorne metric. The left panel corresponds to fixed $q = 0$ and arbitrary $j$, while the right panel represents fixed $j = 0$ and arbitrary $q$. In the left panel, it is evident that the energy of particles for $j > 0$ ($j < 0$) cases is relatively lower (higher) than in the Schwarzschild case. We observe a similarity between the behavior of $E^*$ for co-rotating and counter-rotating orbits in the Kerr spacetime (77). On the right panel, the curve of $E^*$ for the Schwarzschild case is below the curves of $q > 0$ cases, resembling the behavior observed in the $q$-metric with $q > 0$ case or the Kerr metric with counter-rotating orbits (77). In Fig. 6.4, we illustrate the dependence of the normalized ISCO radius $R_{ISCO}/M$ in terms of $j$ and $q$. The left panel shows $R_{ISCO}/M$ versus $q$ for fixed values of $j$. Here, counter-rotating orbits will have larger $R_{ISCO}/M$ with respect to the Schwarzschild (black solid straight line) for increasing $q$. However, co-rotating orbits will

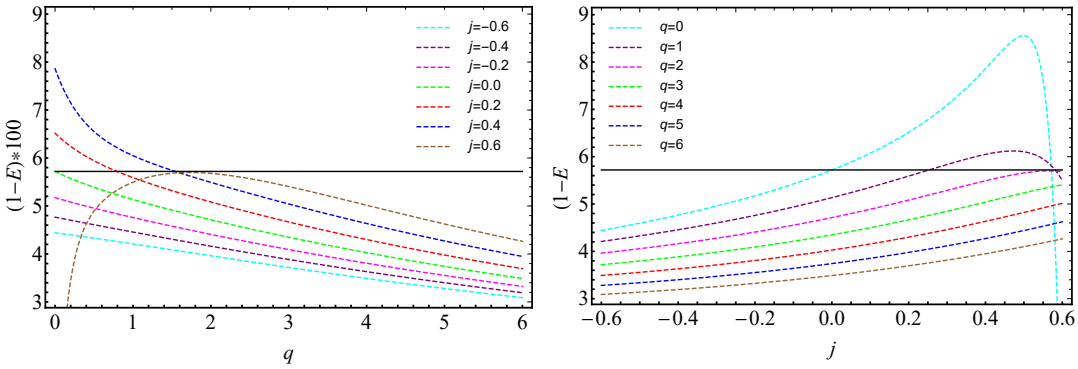


**Figure 6.5:** Efficiency $\eta$ of converting matter into radiation in the Hartle-Thorne spacetime. Left panel: $\eta$ versus $q$ for different values of $j$. Right panel: $\eta$ versus $j$ for different values of $q$.

have smaller $R_{ISCO}/M$ with respect to the Schwarzschild case (black solid straight line) for decreasing $q$. The right panel presents $R_{ISCO}/M$ versus $j$ for fixed values of $q$. Counter-rotating orbits will have larger $R_{ISCO}/M$ with respect to the Schwarzschild (solid straight line) for any value of $q$, but for co-rotating orbits $R_{ISCO}/M$ will be smaller with respect to the Schwarzschild case for small values of $q$. The two panels complement each other. One can see that $R_{ISCO}/M$ in the field of rotating neutron stars with large $j$ can be smaller than in the field of a static neutron star or a Schwarzschild black hole with equal masses. This tendency can be explained by the fact that for small values of $q$ the effects of $j$ start prevailing and the Hartle-Thorne metric behaves like the Kerr metric. Correspondingly, one can observe a similar effect for both co-rotating and counter-rotating orbits in the Kerr spacetime.

In Fig. 6.5, the efficiency of the compact object is illustrated in the Hartle-Thorne spacetime. Left panel shows that for increasing $q$ the efficiency decreases for different values of $j$ and starting from certain values of $q$ the efficiency becomes smaller than in the Schwarzschild case (black solid straight line). Instead, for smaller values of $q$ the efficiency of neutron stars for co-rotating orbits can be larger than the one of a static neutral black hole, possessing the same mass. Here again as in a previous case for small $q$ the effects of $j$ are more dominant. Therefore the trend of the curves are similar to the ones of the Kerr metric for co-rotating orbits. Right panel shows efficiency versus $j$ for $q \geq 0$. As expected for small $q$ and large $j$ the efficiency will be larger than for the Schwarzschild black hole (black solid straight line).

## 6.3 Spectra of thin accretion disks

To investigate the luminosity and spectral characteristics of the accretion disk in the Hartle-Thorne spacetime, we adopt the simplest model for accretion disk, developed by Novikov-Thorne and Page-Thorne as described in Refs. (49; 50). The underlying relativistic models for accretion disks around black holes are limited in their validity and physical realism at the inner edge due to the boundary condition that requires a sudden cessation of viscous stresses at the radius separating the region of circular orbits from the region of spiral orbits.

However, in the case of accreting black holes, emission from the inner disk provides insights into the corresponding black hole spin. According to the model, for a thin accretion disk around a black hole, the accreting matter gradually moves inward along nearly Keplerian orbits due to viscous evolution until it reaches the radius of the innermost stable circular orbit (ISCO), beyond which the gas rapidly falls into the black hole.

Consequently, the inner edge of the viscous accretion disk is predicted to be very close to the ISCO. In this respect, most analytical models of accretion disks assume a stationary and axially symmetric state of the matter being accreted into the black hole. In these scenarios, all physical quantities depend only on two spatial coordinates: the radial distance from the center and the vertical distance from the equatorial symmetry plane.

Even though commonly studied models assume that the disk is not significantly vertically extended, the Novikov-Thorne solution represents local solutions and introduces an assumption that the viscous torque vanishes at the ISCO, leading to a singularity in the model at that point.

For very low accretion rates, this singularity does not significantly affect the electromagnetic spectrum or several other important astrophysical predictions of the model. However, in certain astrophysical scenarios where the inner boundary condition plays a crucial role, such as global modes of disk oscillations, the Novikov-Thorne model is inadequate.

In the subsequent analysis, we make the assumption of a constant mass accretion rate of the disk to meet the aforementioned criteria. Therefore, the primary quantities that describe the model locally are the radiative flux $\mathcal{F}$ and the differential luminosity, which represents the energy per unit time reaching an observer located at infinity, denoted as $\mathcal{L}_\infty$. The differential luminosity $\mathcal{L}_\infty$ is estimated based on the flux $\mathcal{F}$, which represents the energy radiated per unit area per unit time by the accretion disk. The flux definition can be mod-

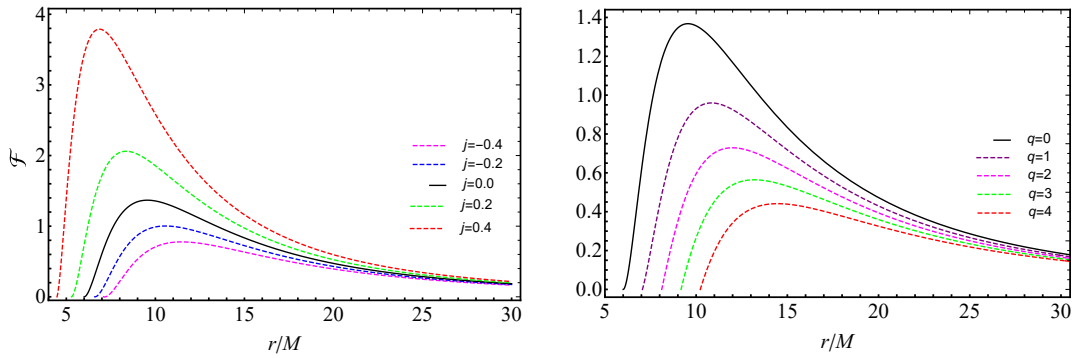


**Figure 6.6:** Radiative flux $\mathcal{F}^*$ multiplied by $10^5$ of the accretion disk in the Hartle-Thorne metric versus radial distance $r$ normalized by the total mass $M$. Left panel: $\mathcal{F}^*$ versus $r/M$ for fixed $q = 0$ and arbitrary $j$. Right panel: $\mathcal{F}^*$ versus $r/M$ for fixed $j = 0$ and arbitrary $q \geq 0$.

ified conveniently. Later, we take its normalized version with respect to total mass $M$, say $\mathcal{F}^*(r) = M^2\mathcal{F}(r)$. Suitably this will help in formulating spectral properties of the disk. We thus have (49; 50)

$$\mathcal{F}(r) = -\frac{\dot{m}}{4\pi\sqrt{-g}}\frac{\Omega_{,r}}{(E-\Omega L)^2}\int_{r_i}^{r}(E-\Omega L)\,L_{,\tilde{r}}d\tilde{r}, \tag{6.3.1}$$

and

$$\frac{d\mathcal{L}_\infty}{d\ln r} = 4\pi r\sqrt{-g}E\mathcal{F}(r), \tag{6.3.2}$$

where in the previous discussion, the term flux refers to the energy radiated per unit area per unit time by the accretion disk.

In the given expression, $r_i = R_{ISCO}$ represents the value of the radial coordinate corresponding to the innermost stable circular orbit (ISCO), while $\dot{m}$ denotes the mass accretion rate of the disk, which is assumed to be constant throughout the analysis. Lastly, $g$ represents the determinant of the metric tensor in the three-dimensional subspace spanned by the coordinates $(t, r, \varphi)$. In the above relation, the effect of the geometry enters through $g$, namely the determinant of the metric of the three-dimensional sub-space $(t, r, \varphi)$ (i.e. $\sqrt{-g} = \sqrt{-g_{rr}(g_{tt}g_{\varphi\varphi} - g_{t\varphi}^2)}$ (78).

### 6.3.1 Emitting properties

The radiative flux and its local definition at infinity represent the radiation emitted by the disk as a function of the radial coordinate. However, they do not consider the measured quantities that involve the spectrum of light and its frequencies.

In practice, we observe the emitted spectrum as a function of frequency. Therefore, it is natural to consider the determination of the spectral luminosity distribution observed at infinity, denoted as $\mathcal{L}_{\nu,\infty}$. Assuming that the overall emission follows a black body radiation pattern and considering $u^t$, the contra-variant time component of the four velocity and $\nu$, the frequency of the emitted radiation, we can handle for the $\mathcal{L}_{\nu,\infty}$ the following formula (79):

$$\nu\mathcal{L}_{\nu,\infty} = \frac{60}{\pi^3}\int_{r_i}^{\infty}\frac{\sqrt{-g}E}{M^2}\frac{(u^t y)^4}{\exp\left[u^t y/\mathcal{F}^{*1/4}\right]-1}dr, \tag{6.3.3}$$

with the positions

$$u^t(r) = \frac{1}{\sqrt{-g_{tt}-2\Omega g_{t\varphi}-\Omega^2 g_{\varphi\varphi}}}, \tag{6.3.4a}$$

$$y = h\nu/kT_* \,. \tag{6.3.4b}$$

Besides the clear definitions of $h$ and $k$ as Planck's and Boltzmann's constants respectively, the relation (6.3.3) is also function of the characteristic temperature, $T_*$. This quantity can be obtained adopting the aforementioned approximation of black body. Hence, taking into account the above Stefan-Boltzmann law we immediately obtain

$$\sigma T_*^4 = \frac{1}{4\pi}\frac{\dot{\mathrm{m}}}{M^2}\,, \tag{6.3.5}$$

### 6.3.2 Numerical analysis

We can now proceed with the numerical analysis based on the theoretical predictions derived from our metric and the assumption of a thin disk. As a result, we present the main outcomes of our study in Figures 6.6, 6.7, and

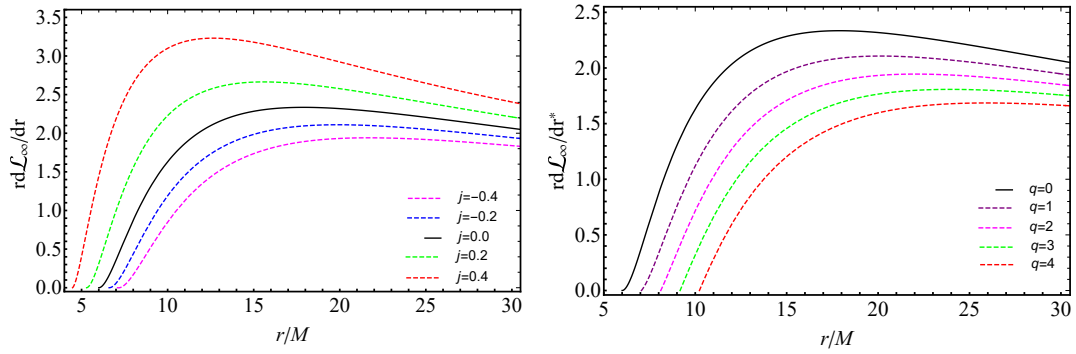


**Figure 6.7:** Differential luminosity multiplied by $10^2$ of the accretion disk in the Hartle-Thorne metric versus radial coordinate $r$ normalized by total mass $M$. Left panel: Differential luminosity versus $r/M$ for fixed $q = 0$ and arbitrary $j$. Right panel: Differential luminosity versus $r/M$ for fixed $j = 0$ and arbitrary $q \geq 0$.

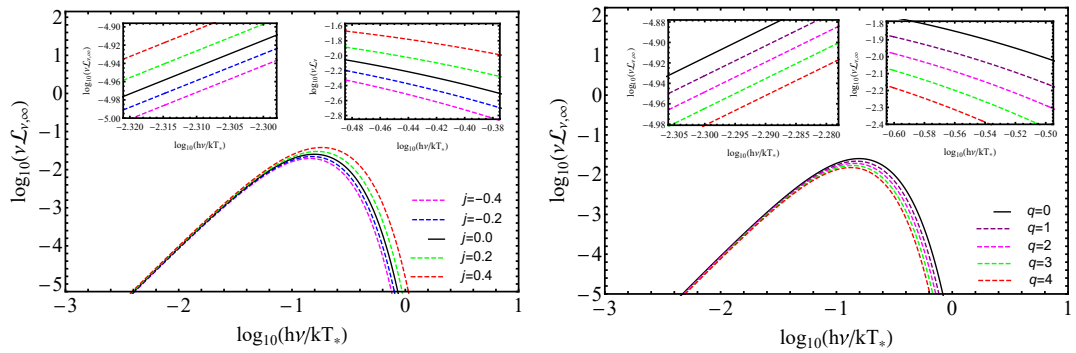


**Figure 6.8:** Spectral luminosity versus frequency of the emitted radiation for blackbody emission of the accretion disk in the Hartle-Thorne metric. Left panel: Spectral luminosity versus frequency for fixed $q = 0$ and arbitrary $j$. Right panel: Spectral luminosity versus frequency for fixed $j = 0$ and arbitrary $q \geq 0$.

6.8. These results can also be compared with previous findings available in the literature.

In the following, we highlight the key characteristics of our study and, specifically,

- Fig. 6.6 showcases the flux distribution, which provides insights into the amount of radiation emitted by the disk as a function of the radial coordinate.

- Fig. 6.7 illustrates the differential luminosity, representing the energy per unit time that reaches an observer located at infinity. This quantity is crucial in understanding the overall energy output of the accretion disk.

- Fig. 6.8 displays the spectral luminosity distribution, denoted as $\mathcal{L}_{\nu,\infty}$. It characterizes the energy emitted by the accretion disk as a function of the frequency of radiation.

By examining these figures, we can gain valuable insights into the behavior and properties of the accretion disk, while also comparing our findings with existing literature.

In particular, for Fig. 6.6, we underline that

- the left panel corresponds to the case of fixed $q = 0$ and arbitrary $j$. We observe that the flux for the Schwarzschild black hole is consistently lower (higher) than the flux for the Hartle-Thorne metric with $j > 0$ ($j < 0$) in the entire range of the radial distance. The behavior of the flux in the Hartle-Thorne metric is similar to that observed in the Kerr metric for co-rotating (counter-rotating) orbits, as noted in the Ref. (77);

- the right panel shows a comparison of the flux for the Schwarzschild black hole with that of a static and deformed object characterized by $j = 0$ and $q \geq 0$. We find that the flux for the Schwarzschild black hole is always greater than the flux for the static and deformed object. This behavior is consistent with the behavior observed in the Kerr metric but for counter-rotating orbits, as indicated in the reference (77);

- these results provide valuable insights into the radiative flux behavior in the Hartle-Thorne metric, and they demonstrate similarities and differences with respect to other metrics, such as the Kerr metric, for various orbit configurations.

From the analysis of the radiative flux, differential luminosity, and the spectral luminosity of the accretion disk, we show that the gravity of a rotating deformed compact object, e.g. neutron star is conceptually different from those of black holes and naked singularities, though occasionally they can display similar features.

Concerning Fig. 6.7, we highlight that

- we present the plot of the differential luminosity as a function of the normalized radial coordinate in the Hartle-Thorne metric. The left panel corresponds to the case of fixed $q = 0$ and arbitrary $j$, while the right panel represents the case of fixed $j = 0$ and arbitrary $q \geq 0$. As the differential luminosity is directly defined in terms of the flux, we notice that the behavior observed in Fig. 6.6 naturally translates into the behavior of the differential luminosity. The left panel of Fig. 6.7 reflects the same trends observed in the left panel of Fig. 6.6, with the differential luminosity for the Hartle-Thorne metric exceeding (not exceeding) for $j > 0$ ($j < 0$) that of the Schwarzschild black hole throughout the radial distance range;

- similarly, the right panel of Fig. 6.7 reflects the behavior observed in the right panel of Fig. 6.6. Here, we compare the differential luminosity for the Hartle-Thorne metric, characterized by $j = 0$ and $q \geq 0$, with that of a Schwarzschild metric (black solid curve). The results show that the differential luminosity for the Schwarzschild metric surpasses that of the Hartle-Thorne metric with $j = 0$ and $q \geq 0$, describing gravitational fields of static and deformed objects;

- these findings highlight the connection between the flux and the differential luminosity, confirming that the behavior observed in Fig. 6.6 is accurately translated into the differential luminosity as well.

While, finally, for Fig. 6.8,

- we present the plot of the spectral luminosity $\mathcal{L}_{\nu,\infty}$ as a function of the frequency of radiation emitted by the accretion disk in the Hartle-Thorne metric. The left panel corresponds to the case of fixed $q = 0$, while the right panel represents the case of fixed $j = 0$.

- Similar to the spectral luminosity obtained using the Kerr metric for co-rotating and counter-rotating orbits, as referenced (79; 77), we observe a

similar pattern in the left and right panels of Fig. 6.8. This indicates that the spectral luminosity in the Hartle-Thorne metric follows a similar trend as in the Kerr metric for the respective orbit configurations.

- The main physical mechanisms yielding similar results for the radiative flux, differential and spectral luminosities between rotating neutron stars and the Kerr black holes are related to the total mass and radius of neutron stars. The more massive neutron stars possess smaller radii and correspondingly tend to have stronger gravitational field (see Fig. 6.9). In turn, due to stronger fields massive neutron stars try to get more spherical shape despite fast rotation. Hence, the effects of the quadrupole moment in this situation becomes less dominant than the effects of the angular momentum (see Fig. 6.10) and the characteristics of the accretion disks around the fast spinning neutron stars become similar to those of around the Kerr black holes.

- Furthermore, it is noteworthy that the spectral luminosity of the accretion disk with $q = 0$ and $j > 0$ ($j < 0$) (left panel) is always larger (smaller) than that in the Schwarzschild spacetime. Conversely, for the case of $j = 0$ and $q \geq 0$ (right panel), the spectral luminosity is always smaller than in the Schwarzschild spacetime.

- These results highlight the differences in spectral luminosity between the Hartle-Thorne metric and the Schwarzschild spacetime, reaffirming the influence of the Hartle-Thorne metric parameters on the emitted radiation from the accretion disk.

## 6.4 Neutron star models

In this section, we examine models of neutron stars and calculate feasible parameters for $M$, $j$, and $q$ using the Hartle-Thorne formalism. We establish that the values of $M$, $j$, and $q$ discussed above align with realistic neutron star models. Furthermore, we illustrate that the radius of ISCO, $R_{ISCO}$, can surpass the size of a neutron star.

### 6.4.1 Mass-radius relations for neutron stars

To determine the mass-radius relationship for neutron stars, it is necessary to select an equation of state and subsequently solve the Tolman-Oppenheimer-Volkoff equation, which describes a static neutron star in hydrostatic equilibrium. This straightforward method becomes more intricate when considering the rotation of a star. Fortunately, there exist established methodologies and publicly accessible numerical codes both in the literature and on dedicated websites, simplifying the process. These resources offer valuable tools for studying the properties and characteristics of rotating neutron stars, see e.g. (45; 68; 80). While the technical aspects of studying neutron stars may be relatively clear, the conceptual challenges arise when considering the equation of state.

Neutron stars are extraordinary objects characterized by extreme densities, pressures, temperatures, electromagnetic fields, and gravitational fields. Unfortunately, these extreme conditions cannot be replicated or reproduced in laboratory settings. Consequently, the equation of state for neutron stars remains an area of ongoing research and is not yet firmly established. The equation of state describes the relationship between various properties of matter within a neutron star, such as density, pressure, temperature, composition etc. Understanding and accurately modeling these relationships is crucial for comprehending the internal structure and behavior of neutron stars. Despite significant progress, the equation of state for neutron stars remains an active area of research and a subject of ongoing debate and investigation and, so, determining an equation of state that accurately represents the complex physics at play is a challenging task.

There are a lot of uncertainties at supra-nuclear densities (22; 24; 27) and this fact generates various models (81; 82; 83; 84; 85; 86), accounting for different processes in neutron stars' crusts (87; 88). In this work we adopt the neutron star model formulated in Ref. (89). We consider this approach since:

- the model or equation of state takes into account strong interaction (based on the Boguta-Bodmer model (90)), weak interaction (taking into account the $\beta$-equilibrium), electromagnetic and gravitational interactions by solving the Einstein-Maxwell-Thomas-Fermi system of equations;

- the equation of state fulfills the global charge neutrality condition, unlike other equations of state which are mainly derived to satisfy the local

charge neutrality condition;

- the equation of state fulfills both theoretical and observational constraints

These are the main reason and motivations to exploit this model. Certainly, it should be stressed that one can refer to any model in the literature. In order to show that our findings are compatible with neutron star physics, and to estimate the basic parameters of neutron stars we adopt here the above mentioned model.

Hence, to construct the mass-radius, mass-central density, radius-central density and other relation we exploit the well-corroborated Hartle's formalism (91; 55).

Specifically, in Fig. 6.9, the mass-radius relation is shown along with observational constraints. The neutron star model we adopted fully satisfies the observational and theoretical constraints, which are listed below. For additional details, see e.g. (29).

In the future, it is anticipated that we may observe more massive neutron stars, as both theoretical static and rotating masses have already exceeded the maximum observed mass. These potential discoveries could provide valuable insights into the nature of neutron star equations of state, particularly those characterized by stiffness or super stiffness (92). By studying these extreme objects, we can gain a deeper understanding of the fundamental properties of matter under extreme conditions, pushing the boundaries of our knowledge in the field of astrophysics.

### 6.4.2 Theoretical and observational constraints

In order to construct realistic and physically self-consistent neutron star models, certain constraints, both theoretical and observational, must be satisfied. Theoretical constraints are derived from fundamental principles and govern the maximum mass of a neutron star, as defined by the Tolman-Oppenheimer-Volkoff limit. However, this limit is model-dependent and needs to be considered in conjunction with observational constraints on neutron star masses (93; 94; 95; 96). Another important theoretical constraint is related to the speed of sound in the extremely dense matter within a neutron star (97). To satisfy the causality principle, the speed of sound must not exceed the speed of light in vacuum. For rotating neutron stars with crusts, there exists

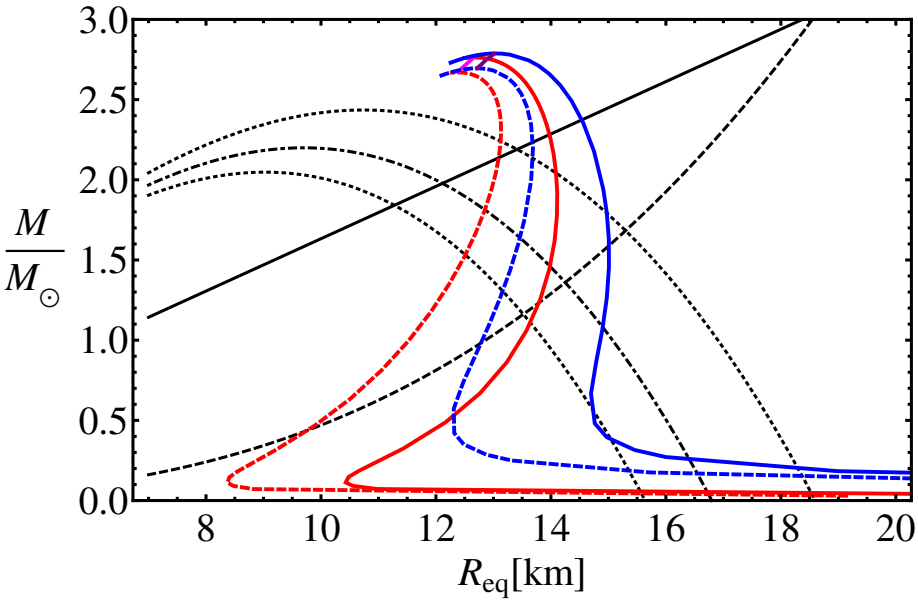


**Figure 6.9:** The mass-radius relations for neutron stars. Dashed/solid blue and red curves indicate static/rotating local charge neutrality (LCN) and global charge neutrality (GCN) cases, respectively. The solid line is the upper limit of the surface gravity of XTE J1814-338, the dotted-dashed curve show the lower limit to the radius of RX J1856-3754, the dashed line is the constraint imposed by the fastest rotating pulsar PSR J1748-2246ad and the dotted curves are the 90 % confidence level contours of constant $R_\infty$ of the neutron star in the low mass X-Ray binary X7. Any realistic mass-radius relation should pass through the area delimited by the solid, the dashed and the dotted lines and in addition it must have a maximum mass larger than the mass of PSR J0740+6620, $M = (2.14 \pm 0.2) M_\odot$.

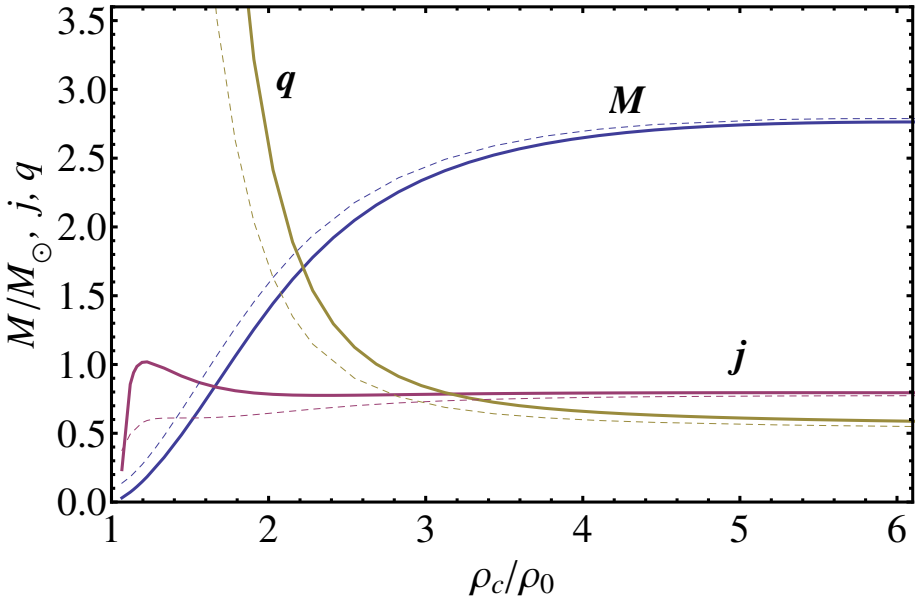


**Figure 6.10:** The mass in solar masses ($M/M_\odot$), the dimensionless angular momentum $j$ and quadrupole moment $q$ as a function of the central density of a maximally rotating neutron star. Solid curves indicate GCN and dashed curves indicate LCN cases.

a constraint on the spin parameter $j$, which should not exceed 0.7 (98). However, for crustless neutron stars, the spin parameter can approach or even exceed unity (99). In our adopted neutron star model, we encounter similar circumstances, where locally neutral neutron stars exhibit properties akin to those with crusts, while globally neutral neutron stars resemble those without crusts (100).

Observational constraints on the mass-radius relations of neutron stars are derived from various measurements, including the largest observed masses (101; 102), the largest observed radii (103), the highest rotational frequencies (82; 104), and the maximum surface gravity (105; 106). These observational constraints play a crucial role in validating and refining our understanding of neutron star properties. For a visual representation, refer to Fig. 6.9.

### 6.4.3 Morphological properties of maximally rotating neutron stars

As an intriguing point, we can now work out the morphological properties of maximally rotating neutron stars, employing the main characteristics of mass, angular momentum and so forth.

In particular, Fig. 6.10 illustrates the key parameters of neutron stars as a function of the central density normalized by the nuclear density ($\rho_0 \approx 2.3 \times 10^{17}$ kg/m$^3$) and,

- the mass, dimensionless angular momentum ($j$), and quadrupole moment ($q$) are depicted for maximally rotating configurations, calculated using the Hartle-Thorne formalism and employing the equation of state described in References (89; 107)

- the plot reveals that as the central density increases, the mass of the neutron star reaches its maximum value, but both $j$ and $q$ decrease. For central densities beyond $\rho_c/\rho_0 \approx 3.4$, the angular momentum parameter $j$ becomes dominant over the quadrupole moment parameter $q$. This intriguing effect suggests that as the central density of a neutron star increases, it becomes more spherical in shape but rotates at a faster rate;

- on the other hand, at lower density ranges, the influence of the quadrupole moment $q$ becomes more pronounced than that of $j$. Consequently, rotating and more massive neutron stars exhibit similarities to Kerr black holes.

In addition, Fig. 6.11 presents the relation between the radius and central density of neutron stars, including the $R_{ISCO}$ and,

- in the case of a static neutron star, the equatorial radius $R_{eq}$ corresponds to the static radius $R_0$. However, starting from a central density of approximately $\rho_c/\rho_0 \approx 2.2$, which corresponds to a neutron star with a mass of approximately $2M_\odot$, the static radius $R_0$ becomes smaller than the innermost stable circular orbit radius $R^0_{ISCO}$. This implies that when measuring $R^0_{ISCO}$, or alternatively the flux and luminosity, it becomes challenging to distinguish between massive neutron stars and low-mass static black holes. To differentiate a massive neutron star from a black hole, one possibility is to observe the photon sphere, which can provide distinctive features;

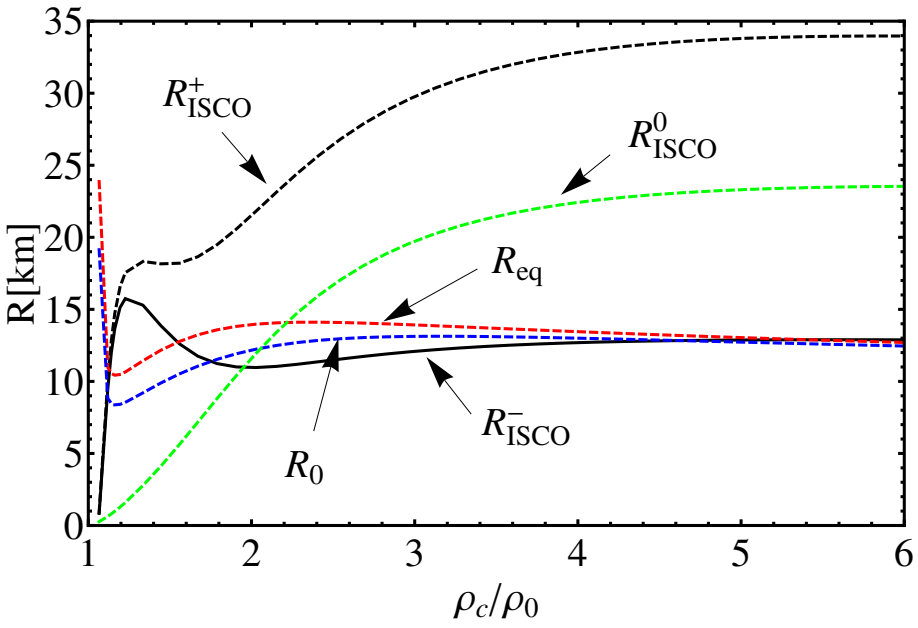


**Figure 6.11:** Different radii as a function of the normalized central density for neutron stars. Where $R^-_{ISCO}/R^+_{ISCO}$ are the ISCO radii for prograde/retrograde orbits, $R_{eq}$ is the equatorial radius of maximally rotating NSs, $R_0$ is the static radius for spherical non-rotating NSs, and $R^0_{ISCO} = 6M$ with $M$ being the static mass of NSs.

- regarding the innermost stable circular orbit radius for co-rotating disks ($R^{-}_{ISCO}$), if a neutron star rotates rapidly, $R^{-}_{ISCO}$ tends to shrink towards the surface of the star. Only for higher central densities does it become slightly larger than the equatorial radius ($R_{eq}$) and exhibit comparable characteristics to a rotating black hole;

- on the other hand, for counter-rotating disks, the innermost stable circular orbit radius ($R^{+}_{ISCO}$) is larger than $R_{eq}$ and $R^{0}_{ISCO}$. It is worth noting that, from a theoretical point of view, counter-rotating disks may exist. However, they are less likely and viable due to the frame-dragging effect near relativistic objects such as neutron stars and black holes. The presence of counter-rotating accretion disks around compact objects remains a topic of ongoing research and investigation.

Finally, it is worth noting that in Figs. 6.11, 6.10 and 6.9 we considered maximally rotating neutron stars, but most of the observed neutron stars and pulsars do not rotate so fast as theoretically estimated (29). Therefore, for slowly rotating stars $j$, $q$ are quite small, and $R^{-}_{ISCO}$ can be close to $R^{0}_{ISCO}$ i.e. outside a neutron star. This implies only one thing that the values of $j$ and $q$ we used above are sufficiently realistic.

## 6.5 Final outlooks and perspectives

In the present work, we investigated the motion of neutral test particles in the Hartle-Thorne spacetime by considering equatorial circular geodesics and examining the influence of the central object angular momentum and quadrupole moment.

We computed important orbital parameters, including angular velocity, angular momentum, and energy for neutral test particles on circular orbits. These quantities exhibited smaller (larger) values for $q = 0$ and $j > 0$ ($j < 0$), ($j = 0$ and $q > 0$) compared with the Schwarzschild case. The ISCO radius was also estimated, and we calculated the efficiency of matter-to-radiation conversion for different values of $j$ and $q$. Our results showed that highly rotating and less deformed objects were more efficient in converting matter into radiation than the Schwarzschild black hole of the same mass, and vice versa.

Using the Novikov-Page-Thorne thin accretion disk model, we determined the radiative flux, differential luminosity, and spectral luminosity. Contrary

to angular velocity, angular momentum, and energy, these quantities exhibited larger (smaller) values for $q = 0$ and $j > 0$, ($j < 0$) ($j = 0$ and $q > 0$) compared with the Schwarzschild case.

Afterwards, we employed a neutron star model described in Refs. (89; 29) to calculate various key parameters of rotating neutron stars, including mass-radius relations, mass-central density relations, radius-central density relations, angular momentum, and quadrupole moment. We compared the ISCO radius with realistic neutron star radii and found that for slowly rotating massive neutron stars, the ISCO radius lies outside the star. Furthermore, we demonstrated that the values of $j$ and $q$ utilized in our study are realistic and consistent with neutron star physics.

Our findings exhibited strong compatibility with configurations incorporating quadrupole effects, obviating the need for additional rotational parameters. However, our results aligned more closely with the Kerr spacetime compared to other metrics. Notably, the $q$-metric failed to reproduce comparable outcomes to the Hartle-Thorne spacetime.

In view of these remarkable results, we intend to further investigate this metric and explore other properties that display notable distinctions from metrics employing quadrupole effects. In particular, involving more accurate accretion disk models and the Hartle-Thorne spacetime would help in shedding light on the role played by quadrupole moments in compact object physics.

# Bibliography


[1] H. Stephani, D. Kramer, M. MacCallum, C. Hoenselaers, and E. Herlt, Exact solutions of Einstein's field equations, Cambridge University Press, Cambridge UK, 2003.

[2] F. J. Ernst, *New formulation of the axially symmetric gravitational field problem*, *Phys. Rev.* **167** (1968) 1175; F. J. Ernst, *New Formulation of the axially symmetric gravitational field problem II* Phys. Rev. **168** (1968) 1415.

[3] H. Quevedo and B. Mashhoon, *Exterior gravitational field of a rotating deformed mass*, *Phys. Lett. A* **109** (1985) 13; H. Quevedo, *Class of stationary axisymmetric solutions of Einstein's equations in empty space*, *Phys. Rev. D* **33** (1986) 324; H. Quevedo and B. Mashhoon, *Exterior gravitational field of a charged rotating mass with arbitrary quadrupole moment*, *Phys. Lett. A* **148** (1990) 149; H. Quevedo, Multipole Moments in General Relativity - Static and Stationary Solutions-, *Fort. Phys.* **38** (1990) 733; H.Quevedo and B. Mashhoon *Generalization of Kerr spacetime*, *Phys. Rev. D* **43** (1991) 3902.

[4] H. Weyl, *Zur Gravitationstheorie*, *Ann. Physik (Leipzig)* **54** (1917) 117.

[5] T. Lewis, *Some special solutions of the equations of axially symmetric gravitational fields*, *Proc. Roy. Soc. London* **136** (1932) 176.

[6] A. Papapetrou, *Eine rotationssymmetrische Lösung in de Allgemeinen Relativitätstheorie*, *Ann. Physik (Leipzig)* **12** (1953) 309.

[7] F. J. Hernandez, F. Nettel, and H. Quevedo, *Gravitational fields as generalized string models*, Grav. Cosmol. **15**, 109 (2009).

[8] H. Quevedo, *General Static Axisymmetric Solution of Einstein's Vacuum Field Equations in Prolate Spheroidal Coordinates*, Phys. Rev. D **39**, 2904–2911 (1989).

[9] G. Erez and N. Rosen, Bull. Res. Counc. Israel **8**, 47 (1959).

[10] B. K. Harrison, Phys. Rev. Lett. **41**, 1197 (1978).

[11] H. Quevedo, *Generating Solutions of the Einstein–Maxwell Equations with Prescribed Physical Properties*, Phys. Rev. D **45**, 1174–1177 (1992).

[12] W. Dietz and C. Hoenselaers, *Solutions of Einstein's equations: Techniques and results*, (Springer Verlag, Berlin, 1984).

[13] V. A. Belinski and V. E. Zakharov, Soviet Phys. – JETP, **50**, 1 (1979).

[14] C. W. Misner, *Harmonic maps as models for physical theories*, *Phys. Rev. D* **18** (1978) 4510.

[15] D. Korotkin and H. Nicolai, *Separation of variables and Hamiltonian formulation for the Ernst equation*, *Phys. Rev. Lett.* **74** (1995) 1272.

[16] J. Polchinski, String Theory: An introduction to the bosonic string, Cambridge University Press, Cambridge, UK, 2001.

[17] D. Nuñez, H. Quevedo and A. Sánchez, *Einstein's equations as functional geodesics*, *Rev. Mex. Phys.* **44** (1998) 440; J. Cortez, D. Nuñez, and H. Quevedo, *Gravitational fields and nonlinear sigma models*, *Int. J. Theor. Phys.* **40** (2001) 251.

[18] R. Geroch, *J. Math. Phys.* **11**, 2580 (1970).

[19] R. O. Hansen, *J. Math. Phys.* **15**, 46 (1974).

[20] D. Bini, A. Geralico, O. Luongo, and H. Quevedo, *Generalized Kerr spacetime with an arbitrary quadrupole moment: Geometric properties vs particle motion*, Class. Quantum Grav. **26**, 225006 (2009).

[21] K. Boshkayev et al. *Accretion disk in the Hartleâ€"Thorne spacetime*, Eur. Phys. J. Plus **139**, 273 (2024).

[22] Zeldovich, Y.B., Novikov, I.D.: Relativistic Astrophysics. Vol.1: Stars and Relativity. University of Chicago Press, Chicago (1971)

[23] Misner, C.W., Thorne, K.S., Wheeler, J.A.: Gravitation. W. H. Freeman and Company, San Francisco (1973)

[24] Shapiro, S.L., Teukolsky, S.A.: Black Holes, White Dwarfs and Neutron Stars. Wiley-VCH, New York (1983). 10.1002/9783527617661

[25] Ohanian, H.C., Ruffini, R.: Gravitation and Spacetime. 3rd Edition, Cambridge University Press, Cambridge (2013)

[26] Chruściel, P.T., Costa, J.L., Heusler, M.: Stationary Black Holes: Uniqueness and Beyond. Living Reviews in Relativity 15(1), 7 (2012) 10.12942/lrr-2012-7 arXiv:1205.6112 [gr-qc]

[27] Haensel, P., Potekhin, A.Y., Yakovlev, D.G. (eds.): Neutron Stars 1 : Equation of State and Structure. Astrophysics and Space Science Library, vol. 326 (2007)

[28] Boshkayev, K., Rueda, J.A., Ruffini, R., Siutsou, I.: On General Relativistic Uniformly Rotating White Dwarfs. 762(2), 117 (2013) 10.1088/0004-637X/762/2/117 arXiv:1204.2070 [astro-ph.SR]

[29] Belvedere, R., Boshkayev, K., Rueda, J.A., Ruffini, R.: Uniformly rotating neutron stars in the global and local charge neutrality cases. 921, 33–59 (2014) 10.1016/j.nuclphysa.2013.11.001 arXiv:1307.2836 [astro-ph.SR]

[30] Torres, D.F.: Accretion disc onto a static non-baryonic compact object. Nuclear Physics B 626(1-2), 377–394 (2002) 10.1016/S0550-3213(02)00038-X arXiv:hep-ph/0201154 [hep-ph]

[31] Guzmán, F.S.: Accretion disk onto boson stars: A way to supplant black hole candidates. 73(2), 021501 (2006) 10.1103/PhysRevD.73.021501 arXiv:gr-qc/0512081 [gr-qc]

[32] Beheshti, S., Gasperín, E.: Marginally stable circular orbits in stationary axisymmetric spacetimes. 94(2), 024015 (2016) 10.1103/PhysRevD.94.024015 arXiv:1512.08707 [gr-qc]

[33] Cardoso, V., Pani, P.: Testing the nature of dark compact objects: a status report. Living Reviews in Relativity 22(1), 4 (2019) 10.1007/s41114-019-0020-4 arXiv:1904.05363 [gr-qc]

[34] Mazur, P.O., Mottola, E.: Gravitational vacuum condensate stars. Proceedings of the National Academy of Science 101(26), 9545–9550 (2004) 10.1073/pnas.0402717101 arXiv:gr-qc/0407075 [gr-qc]

[35] Gravity Collaboration: Detection of the gravitational redshift in the orbit of the star S2 near the Galactic centre massive black hole. 615, 15 (2018) 10.1051/0004-6361/201833718 arXiv:1807.09409 [astro-ph.GA]

[36] Ghez, A.M., Klein, B.L., Morris, M., Becklin, E.E.: High Proper-Motion Stars in the Vicinity of Sagittarius A*: Evidence for a Supermassive Black Hole at the Center of Our Galaxy. 509(2), 678–686 (1998) 10.1086/306528 arXiv:astro-ph/9807210 [astro-ph]

[37] Ghez, A.M., Morris, M., Becklin, E.E., Tanner, A., Kremenek, T.: The accelerations of stars orbiting the Milky Way's central black hole. 407(6802), 349–351 (2000) 10.1038/35030032 arXiv:astro-ph/0009339 [astro-ph]

[38] Remillard, R.A., McClintock, J.E.: X-Ray Properties of Black-Hole Binaries. 44(1), 49–92 (2006) 10.1146/annurev.astro.44.051905.092532 arXiv:astro-ph/0606352 [astro-ph]

[39] Abbott, B.P.e.: Observation of Gravitational Waves from a Binary Black Hole Merger. 116(6), 061102 (2016) 10.1103/PhysRevLett.116.061102 arXiv:1602.03837 [gr-qc]

[40] Abbott, B.P.e.: Tests of General Relativity with GW150914. 116(22), 221101 (2016) 10.1103/PhysRevLett.116.221101 arXiv:1602.03841 [gr-qc]

[41] Event Horizon Telescope Collaboration: First M87 Event Horizon Telescope Results. I. The Shadow of the Supermassive Black Hole. 875(1), 1 (2019) 10.3847/2041-8213/ab0ec7 arXiv:1906.11238 [astro-ph.GA]

[42] Abishev, M., Boshkayev, K., Quevedo, H., Toktarbay, S.: Accretion disks around a mass with quadrupole. In: Hsu, J.-P., (eds.) Gravitation, Astrophysics, and Cosmology, p. 185 (2016). 10.1142/9789814759816_0026

[43] Abramowicz, M.A., Fragile, P.C.: Foundations of Black Hole Accretion Disk Theory. Living Reviews in Relativity 16(1), 1 (2013) 10.12942/lrr-2013-1 arXiv:1104.5499 [astro-ph.HE]

[44] Andersson, N., Comer, G.L.: Slowly rotating general relativistic superfluid neutron stars. Classical and Quantum Gravity 18(6), 969–1002 (2001) 10.1088/0264-9381/18/6/302 arXiv:gr-qc/0009089 [gr-qc]

[45] Stergioulas, N.: Rotating Stars in Relativity. Living Reviews in Relativity 6(1), 3 (2003) 10.12942/lrr-2003-3 arXiv:gr-qc/0302034 [gr-qc]

[46] Berti, E., Stergioulas, N.: Approximate matching of analytic and numerical solutions for rapidly rotating neutron stars. 350(4), 1416–1430 (2004) 10.1111/j.1365-2966.2004.07740.x arXiv:gr-qc/0310061 [gr-qc]

[47] Berti, E., White, F., Maniopoulou, A., Bruni, M.: Rotating neutron stars: an invariant comparison of approximate and numerical space-time models. 358(3), 923–938 (2005) 10.1111/j.1365-2966.2005.08812.x arXiv:gr-qc/0405146 [gr-qc]

[48] Mashhoon, B., Theiss, D.S.: Relativistic lunar theory. Nuovo Cimento B Serie 106(5), 545–571 (1991) 10.1007/BF02726789

[49] Novikov, I.D., Thorne, K.S.: Astrophysics of black holes. In: Black Holes (Les Astres Occlus), p. 343 (1973)

[50] Page, D.N., Thorne, K.S.: Disk-Accretion onto a Black Hole. Time-Averaged Structure of Accretion Disk. 191, 499–506 (1974) 10.1086/152990

[51] Boshkayev, K., Malafarina, D.: A model for a dark matter core at the Galactic Centre. 484(3), 3325–3333 (2019) 10.1093/mnras/stz219 arXiv:1811.04061 [gr-qc]

[52] Kurmanov, E., Boshkayev, K., Giambò, R., Konysbayev, T., Luongo, O., Malafarina, D., Quevedo, H.: Accretion Disk Luminosity for Black Holes Surrounded by Dark Matter with Anisotropic Pressure. 925(2), 210 (2022) 10.3847/1538-4357/ac41d4

[53] Boshkayev, K., Konysbayev, T., Kurmanov, Y., Luongo, O., Malafarina, D.: Accretion Disk Luminosity for Black Holes Surrounded by Dark Matter with Tangential Pressure. 936(2), 96 (2022) 10.3847/1538-4357/ac8804 arXiv:2205.04208 [gr-qc]

[54] Bini, D., Geralico, A., Luongo, O., Quevedo, H.: Generalized Kerr spacetime with an arbitrary mass quadrupole moment: geometric properties versus particle motion. Classical and Quantum Gravity 26(22), 225006 (2009) 10.1088/0264-9381/26/22/225006 arXiv:0909.4150 [gr-qc]

[55] Hartle, J.B., Thorne, K.S.: Slowly Rotating Relativistic Stars. II. Models for Neutron Stars and Supermassive Stars. 153, 807 (1968) 10.1086/149707

[56] Stephani, H., Kramer, D., MacCallum, M., Hoenselaers, C., Herlt, E.: Exact Solutions of Einstein's Field Equations. Cambridge University Press, ??? (2003). 10.1017/CBO9780511535185

[57] Geroch, R.: Multipole Moments. II. Curved Space. Journal of Mathematical Physics 11(8), 2580–2588 (1970) 10.1063/1.1665427

[58] Hansen, R.O.: Multipole moments of stationary space-times. Journal of Mathematical Physics 15(1), 46–52 (1974) 10.1063/1.1666501

[59] Boshkayev, K., Quevedo, H., Nurbakyt, G., Malybayev, A., Urazalina, A.: The Erez–Rosen Solution Versus the Hartle–Thorne Solution. Symmetry 11(10), 1324 (2019) 10.3390/sym11101324 arXiv:1909.10949 [gr-qc]

[60] Frutos-Alfaro, F., Soffel, M.: On the post-linear quadrupole-quadrupole metric. Revista de Matemática: Teoría y Aplicaciones 24, 239–255 (2015) arXiv:1507.04264 [gr-qc]

[61] Boshkayev, K., Malybayev, A., Quevedo, H., Nurbakyt, G., Taukenova, A., Urazalina, A.: The correspondence of the erez-rosen solution with the hartle-thorne solution in the limiting case of $m^2$ and $q$. 5(333), 19–27 (2020)

[62] Quevedo, H., Mashhoon, B.: Exterior gravitational field of a rotating deformed mass. Physics Letters A 109(1-2), 13–18 (1985) 10.1016/0375-9601(85)90381-0

[63] Quevedo, H.: General static axisymmetric solution of Einstein's vacuum field equations in prolate spheroidal coordinates. 39(10), 2904–2911 (1989) 10.1103/PhysRevD.39.2904

[64] Quevedo, H.: Multipole Moments in General Relativity —Static and Stationary Vacuum Solutions—. Fortschritte der Physik 38(10), 733–840 (1990) 10.1002/prop.2190381002

[65] Quevedo, H., Mashhoon, B.: Exterior gravitational field of a charged rotating mass with arbitrary quadrupole moment. Physics Letters A 148(3-4), 149–153 (1990) 10.1016/0375-9601(90)90770-O

[66] Quevedo, H., Mashhoon, B.: Generalization of Kerr spacetime. 43(12), 3902–3906 (1991) 10.1103/PhysRevD.43.3902

[67] Boshkayev, K., Quevedo, H., Ruffini, R.: Gravitational field of compact objects in general relativity. 86(6), 064043 (2012) 10.1103/PhysRevD.86.064043 arXiv:1207.3043 [gr-qc]

[68] Yagi, K., Kyutoku, K., Pappas, G., Yunes, N., Apostolatos, T.A.: Effective no-hair relations for neutron stars and quark stars: Relativistic results. 89(12), 124013 (2014) 10.1103/PhysRevD.89.124013 arXiv:1403.6243 [gr-qc]

[69] Boshkayev, K., Quevedo, H., Toktarbay, S., Zhami, B., Abishev, M.: On the equivalence of approximate stationary axially symmetric solutions of the Einstein field equations. Gravitation and Cosmology 22(4), 305–311 (2016) 10.1134/S0202289316040046 arXiv:1510.02035 [gr-qc]

[70] Allahyari, A., Firouzjahi, H., Mashhoon, B.: Quasinormal modes of a black hole with quadrupole moment. 99(4), 044005 (2019) 10.1103/PhysRevD.99.044005 arXiv:1812.03376 [gr-qc]

[71] Frutos-Alfaro, F., Soffel, M.: On relativistic multipole moments of stationary space-times. Royal Society Open Science 5(7), 180640 (2018) 10.1098/rsos.180640 arXiv:1606.07173 [gr-qc]

[72] Allahyari, A., Firouzjahi, H., Mashhoon, B.: Quasinormal modes of generalized black holes: $\delta$-Kerr spacetime. Classical and Quantum Gravity 37(5), 055006 (2020) 10.1088/1361-6382/ab6860 arXiv:1908.10813 [gr-qc]

[73] Abramowicz, M.A., Almergren, G.J.E., Kluzniak, W., Thampan, A.V.: The Hartle-Thorne circular geodesics. arXiv e-prints, 0312070 (2003) 10.48550/arXiv.gr-qc/0312070 arXiv:gr-qc/0312070 [gr-qc]

[74] Bambi, C., Nampalliwar, S.: Quasi-periodic oscillations as a tool for testing the Kerr metric: A comparison with gravitational waves and iron line. EPL (Europhysics Letters) 116(3), 30006 (2016) 10.1209/0295-5075/116/30006 arXiv:1604.02643 [gr-qc]

[75] Bambi, C., Barausse, E.: Constraining the Quadrupole Moment of Stellar-mass Black Hole Candidates with the Continuum Fitting Method. 731(2), 121 (2011) 10.1088/0004-637X/731/2/121 arXiv:1012.2007 [gr-qc]

[76] Boshkayev, K., Gasperín, E., Gutiérrez-Piñeres, A.C., Quevedo, H., Toktarbay, S.: Motion of test particles in the field of a naked singularity. 93(2), 024024 (2016) 10.1103/PhysRevD.93.024024 arXiv:1509.03827 [gr-qc]

[77] Boshkayev, K., Konysbayev, T., Kurmanov, E., Luongo, O., Malafarina, D., Quevedo, H.: Luminosity of accretion disks in compact objects with a quadrupole. 104(8), 084009 (2021) 10.1103/PhysRevD.104.084009 arXiv:2106.04932 [gr-qc]

[78] Bambi, C.: A Code to Compute the Emission of Thin Accretion Disks in Non-Kerr Spacetimes and Test the Nature of Black Hole Candidates. 761(2), 174 (2012) 10.1088/0004-637X/761/2/174 arXiv:1210.5679 [gr-qc]

[79] Boshkayev, K., Idrissov, A., Luongo, O., Malafarina, D.: Accretion disc luminosity for black holes surrounded by dark matter. 496(2), 1115–1123 (2020) 10.1093/mnras/staa1564 arXiv:2006.01269 [astro-ph.HE]

[80] Cipolletta, F., Cherubini, C., Filippi, S., Rueda, J.A., Ruffini, R.: Fast rotating neutron stars with realistic nuclear matter equation of state. 92(2), 023007 (2015) 10.1103/PhysRevD.92.023007 arXiv:1506.05926 [astro-ph.SR]

[81] Lattimer, J.M., Prakash, M.: Neutron Star Structure and the Equation of State. 550(1), 426–442 (2001) 10.1086/319702 arXiv:astro-ph/0002232 [astro-ph]

[82] Lattimer, J.M., Prakash, M.: The Physics of Neutron Stars. Science 304(5670), 536–542 (2004) 10.1126/science.1090720 arXiv:astro-ph/0405262 [astro-ph]

[83] Lattimer, J.M., Prakash, M.: Neutron star observations: Prognosis for equation of state constraints. 442(1-6), 109–165 (2007) 10.1016/j.physrep.2007.02.003 arXiv:astro-ph/0612440 [astro-ph]

[84] Lattimer, J.M., Prakash, M.: The equation of state of hot, dense matter and neutron stars. 621, 127–164 (2016) 10.1016/j.physrep.2015.12.005 arXiv:1512.07820 [astro-ph.SR]

[85] Pretel, J.M.Z., da Silva, M.F.A.: Stability and gravitational collapse of neutron stars with realistic equations of state. 495(4), 5027–5039 (2020) 10.1093/mnras/staa1493 arXiv:2005.13651 [gr-qc]

[86] Greif, S.K., Hebeler, K., Lattimer, J.M., Pethick, C.J., Schwenk, A.: Equation of State Constraints from Nuclear Physics, Neutron Star Masses, and Future Moment of Inertia Measurements. 901(2), 155 (2020) 10.3847/1538-4357/abaf55 arXiv:2005.14164 [astro-ph.HE]

[87] Takibayev, N., Nasirova, D., Katō, K., Kurmangaliyeva, V.: Excited nuclei, resonances and reactions in neutron star crusts. In: Journal of Physics Conference Series. Journal of Physics Conference Series, vol. 940, p. 012058 (2018). 10.1088/1742-6596/940/1/012058

[88] Takibayev, N., Kurmangaliyeva, V.O., Katō, K., Vasilevsky, V.S.: Few-Body Reactions and Processes in Neutron Star Envelopes, pp. 157–161. Springer, Cham (2020)

[89] Belvedere, R., Pugliese, D., Rueda, J.A., Ruffini, R., Xue, S.-S.: Neutron star equilibrium configurations within a fully relativistic theory with strong, weak, electromagnetic, and gravitational interactions. 883, 1–24 (2012) 10.1016/j.nuclphysa.2012.02.01810.48550/arXiv.1202.6500 arXiv:1202.6500 [astro-ph.SR]

[90] Boguta, J., Bodmer, A.R.: Relativistic calculation of nuclear matter and the nuclear surface. 292(3), 413–428 (1977) 10.1016/0375-9474(77)90626-1

[91] Hartle, J.B.: Slowly Rotating Relativistic Stars. I. Equations of Structure. 150, 1005 (1967) 10.1086/149400

[92] Yakovlev, D.G.: General relativity and neutron stars. International Journal of Modern Physics A 31, 1641017 (2016) 10.1142/S0217751X16410177

[93] Bombaci, I.: The maximum mass of a neutron star. 305, 871 (1996)

[94] Kalogera, V., Baym, G.: The Maximum Mass of a Neutron Star. 470, 61 (1996) 10.1086/310296 arXiv:astro-ph/9608059 [astro-ph]

[95] Demorest, P.B., Pennucci, T., Ransom, S.M., Roberts, M.S.E., Hessels, J.W.T.: A two-solar-mass neutron star measured using Shapiro delay. 467(7319), 1081–1083 (2010) 10.1038/nature09466 arXiv:1010.5788 [astro-ph.HE]

[96] Rezzolla, L., Most, E.R., Weih, L.R.: Using Gravitational-wave Observations and Quasi-universal Relations to Constrain the Maximum Mass of Neutron Stars. 852(2), 25 (2018) 10.3847/2041-8213/aaa401 arXiv:1711.00314 [astro-ph.HE]

[97] Tlemissov, A., Tlemissova, Z., Boshkayev, K., Urazalina, A., Quevedo, H.: Analysis of the equations of state for neutron stars. News of the National Academy of Sciences of the Republic of Kazakhstan. Physical and Mathematical Series 5(333), 43–52 (2020)

[98] Lo, K.-W., Lin, L.-M.: The Spin Parameter of Uniformly Rotating Compact Stars. 728(1), 12 (2011) 10.1088/0004-637X/728/1/12 arXiv:1011.3563 [astro-ph.HE]

[99] Qi, B., Zhang, N.-B., Sun, B.-Y., Wang, S.-Y., Gao, J.-H.: A key factor to the spin parameter of uniformly rotating compact stars: crust structure. Research in Astronomy and Astrophysics 16(4), 60 (2016) 10.1088/1674-4527/16/4/060 arXiv:1408.1654 [astro-ph.SR]

[100] Boshkayev, K., Rueda, J.A., Muccino, M.: Main parameters of neutron stars from quasi-periodic oscillations in low mass X-ray binaries. In: Bianchi, M., Jansen, R.T., Ruffini, R. (eds.) Fourteenth Marcel Grossmann Meeting - MG14, pp. 3433–3440 (2018). $10.1142/9789813226609_0442$

[101] Antoniadis, J.e.: A Massive Pulsar in a Compact Relativistic Binary. Science 340(6131), 448 (2013) 10.1126/science.1233232 arXiv:1304.6875 [astro-ph.HE]

[102] Cromartie, H.T., et.al: Relativistic Shapiro delay measurements of an extremely massive millisecond pulsar. Nature Astronomy 4, 72–76 (2020) 10.1038/s41550-019-0880-2 arXiv:1904.06759 [astro-ph.HE]

[103] Trümper, J.E., Burwitz, V., Haberl, F., Zavlin, V.E.: The puzzles of RX J1856.5-3754: neutron star or quark star? Nuclear Physics B Proceedings Supplements 132, 560–565 (2004) 10.1016/j.nuclphysbps.2004.04.094 arXiv:astro-ph/0312600 [astro-ph]

[104] Hessels, J.W.T., Ransom, S.M., Stairs, I.H., Freire, P.C.C., Kaspi, V.M., Camilo, F.: A Radio Pulsar Spinning at 716 Hz. Science 311(5769), 1901–1904 (2006) 10.1126/science.1123430 arXiv:astro-ph/0601337 [astro-ph]

[105] Heinke, C.O., Rybicki, G.B., Narayan, R., Grindlay, J.E.: A Hydrogen Atmosphere Spectral Model Applied to the Neutron Star X7 in the Globular Cluster 47 Tucanae. 644(2), 1090–1103 (2006) 10.1086/503701 arXiv:astro-ph/0506563 [astro-ph]

[106] Trümper, J.E.: Observations of neutron stars and the equation of state of matter at high densities. Progress in Particle and Nuclear Physics 66(3), 674–680 (2011) 10.1016/j.ppnp.2011.01.018

[107] Boshkayev, K., Rueda, J., Muccino, M.: Extracting multipole moments of neutron stars from quasi-periodic oscillations in low mass X-ray binaries. Astronomy Reports 59(6), 441–446 (2015) 10.1134/S1063772915060050